



## WP1

# Feasibility Study of the Subsurface of Tilburg Area for Eavor-Loop

<b>Project name</b>	ELFO: <u>E</u> avor- <u>L</u> oop <u>F</u> easibility for Tilburg (Amer network) and <u>O</u> utlook for application in the Netherlands	
<b>TKI reference</b>	1921406	
<b>Consortium partners</b>	Eavor, Ennatuurlijk, Huisman, TNO	
<b>Duration</b>	01/11/2021 – 31/01/2023	
<b>Work package</b>	WP1 – Feasibility study of the Subsurface of Tilburg area for Eavor-Loop	
<b>Dissemination level</b>	Public	
<b>Lead author(s)</b>	Stephen Longfield (Eavor), Vincent Soustelle (TNO)	
<b>Contributors</b>	Francesco Vinci (Panterra Geoconsultants), Hans Kol (Eavor), Matthew Seager (Eavor), Chris Cheng (Eavor), Todd Stuebing (Eavor), Jan-Diederik van Wees (TNO)	
<b>Verified (WP leader)</b>	Stephen Longfield (Eavor)	Date: 15/01/2023
<b>Approved (coordinator)</b>	Maartje Koning (TNO)	Date: 31/01/2023
<b>Version</b>	1.0	



*The ELFO project has received funding through Topsector Energy (TKI Urban Energy programme) and these financial contributions are gratefully acknowledged. The contents of this publication reflect only the author's view and do not necessarily reflect the opinion of the funding agencies.*

*Het project is uitgevoerd met PPS-programmatoeslag subsidie van het Ministerie van Economische Zaken en Klimaat voor TKI Urban Energy, Topsector Energie. [www.tki-urbanenergy.nl](http://www.tki-urbanenergy.nl).*

## Executive summary

Eavor Technologies Inc. and its Amsterdam-based, European subsidiary, Eavor Europe B.V. (Eavor) has partnered with Eindhoven-based Ennatuurlijk B.V. and Energie Beheer Nederland B.V. (EBN) to develop an Eavor-Loop project near the city of Tilburg in southern Holland.

The Eavor-Loop is a deep closed-loop geothermal system that is differentiated from other geothermal solutions in that the Eavor-Loop relies only on conductive heat transfer, rather than convection or reservoir fluid flow, and can be thought of as a large closed-loop subsurface radiator. The design removes the need for a hydrothermal source, has minimal water use, eliminates the complex resource characterization cost and time associated with geothermal reservoirs, and provides extremely predictable output.

The scope of the Eavor-Loop Tilburg Project (the Project) is to drill and construct one Eavor-Loop which will generate thermal energy (heat), to be used by Ennatuurlijk as a renewable heat source for the Amer Heat Network. The Eavor-Loop will consist of two vertical wells, each connected to 12 horizontal laterals of 2100 m in length at a depth of 3250 m.

Work Package 1 (WP1) was designed to characterize the subsurface through geological, geophysical, geomechanical and thermodynamic investigation. The resultant geological model identifies the Lower German Triassic as a suitable hot reservoir for Eavor-Loop placement given a depth of 3,250m TVD, a geothermal gradient of 32.4°C/km, a thermal conductivity of 4.40 W/m·K and robust mechanical strength properties as input to WP3.

Given the aforementioned subsurface conditions, the predicted energy yield for the project is 9.1 MW during the summer months and 7.1 MW during the winter months. The Project will be funded by equity contributed by the Project partners as well as a capital grant through the NieuweWarmteNu! (NWN!) program with a set SDE++ energy subsidy to be defined in 2023 by RVO. The assumed construction cost of this Eavor-Loop project is 54.5 MM € with annual operating cost of 0.16 MM €.

In order to meet the temperature requirements of the Amer network, a heat pump will be integrated with the Eavor-Loop system to increase the Eavor-Loop outlet temperature to ensure the heat demand can be met throughout the year. The heat pump used for the Project has a COP of 3.72 and an electrical draw of 667 kW. Project construction is currently forecasted to begin in H2 2024 with a commercial operations date in 2025.

# Contents

<b>1. General</b> .....	<b>7</b>
1.1. Introduction .....	7
1.2. WP1 Goals & Objectives.....	8
1.3. Data availability & uncertainty .....	8
1.3.1. Well Data.....	9
1.3.2. Seismic Data .....	10
<b>2. WP1 Subsurface Feasibility</b> .....	<b>12</b>
2.1. Seismic interpretation.....	12
2.1.1. Method .....	12
2.1.2. Well-to-Seismic Ties .....	12
2.1.3. Seismic Interpretation .....	13
2.1.4. Gridding Algorithm.....	14
2.1.5. Time-Depth Conversion.....	14
2.1.6. Depth Map of Top/Base Formation.....	16
2.1.6.1. Discussion of Uncertainty of Top/Base Formation Map .....	18
2.2. In-situ stress Tilburg area .....	19
2.2.1. Tectonic setting.....	19
2.2.2. In-situ stress South (East) Netherlands .....	19
2.2.3. Implications for the Tilburg area .....	20
2.3. Experimental dataset on mechanical properties of the Volpriehausen Sandstones .....	22
2.3.1. Sample selection .....	22
2.3.1.1. Experimental setup .....	24
2.3.1.2. Measurements of mechanical parameters and thermal expansion coefficient .....	26
2.3.1.3. Experimental procedure:.....	28
2.3.1.4. Experimental results.....	28
2.4. Thermal Conductivity .....	31
2.5. Geothermal Gradient and Heat in Place.....	34
2.6. Subsurface 3D Geological Model .....	36
2.7. Eavor-Loop location & design .....	38
2.7.1. Project Location .....	38
2.7.2. Eavor-Loop Design.....	42
2.8. Thermal output .....	47
2.8.1. Thermal Depletion / Degradation .....	49
2.8.2. P50 Energy Yield.....	49
2.8.3. Surface Facilities and Process Flow Conditions .....	50
2.9. Techno-Economic modelling .....	51
<b>3. WP1 Discussion &amp; Conclusions</b> .....	<b>53</b>
<b>4. References</b> .....	<b>54</b>
<b>Appendix A. Experimental data vs. Time</b> .....	<b>56</b>
<b>Appendix B. Measured elastic Moduli for RBMV samples</b> .....	<b>58</b>

## Tables

Table 1: Selected wells for the study and the purpose for which well data were used. ....	9
Table 2: List of key horizons interpreted for this study and their character .....	14
Table 3: V0 and k parameters used for the time depth conversion .....	15
Table 4: Table showing the depths differences and residuals between wells and time-depth converted grids .....	16
Table 5: Coordinates of Eavor-Loop surface location and targeted top reservoir .....	18
Table 6: Experiments summary.....	24
Table 7: Thermal conductivity estimates for the Main Buntsandstein.....	33
Table 8: Temperature and Depth measurements of Tilburg offset wells indicating range of geothermal gradient values .....	35
Table 9: Comparison of Traditional Geothermal and Eavor-Loop Technology.....	46
Table 10: thermodynamic parameter comparison for Eavor-Lite and Tilburg Loop systems.....	47
Table 11: P50 Output Parameters.....	50
Table 12: Heat Pump Design Specifications .....	51
Table 13: Financial Model Inputs and Outputs .....	52

## Figures

Figure 1: Stylized schematic of the Eavor-Loop planned near Tilburg .....	8
Figure 2: Location of wells and seismic data used in the study.....	10
Figure 3: Geometry of the L3CLY2001A survey (3D_Tilbwaalw_TWT).....	11
Figure 4: Seismic to well tie for HBV-01 .....	13
Figure 5: Base Muschelkalk (Top reservoir) depth structural map based on seismic interpretation (after time-depth conversion). Fault polygons in blue (E-dipping), red (W-dipping), yellow (N-dipping) and green (S-dipping). Orange polygon shows Tilburg AOI, green lines show geothermal licence area. Yellow dots are Top reservoir penetration points. Contour interval is 50 m. ....	16
Figure 6: Base Volpriehausen (Base reservoir) depth structural map based on seismic interpretation (after time-depth conversion). Fault polygons in blue (E-dipping), red (W-dipping), yellow (N-dipping) and green (S-dipping). Orange polygon shows Tilburg AOI, green lines show geothermal license area. Yellow dots are Top Reservoir penetration points (base is not reached). Contour interval is 50m. ...	17
Figure 7: Thickness map of the reservoir (Triassic sandstone) based on seismic interpretation (after time-depth grid conversion). Orange polygon shows Tilburg AOI, green lines show geothermal license area. Yellow dots are Top reservoir penetration points (the base is not reached). Contour interval is 25 m.....	18
Figure 8: Overview of tectonic elements, seismicity and hydrocarbon reservoirs in the Netherlands (source Van Wees et al., 2014). Natural seismicity is shown in red circles, induced seismicity is shown in blue circles (larger events in yellow). Hydrocarbon reservoirs are indicated in green (gas) and red (oil). Major fault zones (solid lines) separate the main tectonic elements which characterize the subsurface of the Netherlands (after Wong et al., 2007). Triangles correspond to Leak off test (LOT). Colors denote different regions: BFB = Broad Fourteen Basin, FP = Friesland Platform, GH/LT = Groningen High/Lauwerszee Trough, LSB = Lower Saxony Basin, LT-HP = Lauwerszee trough-Hantum Platform, NHP = Noord Holland Platform, WNB =West Netherlands Basin. RVG = Roer Valley Graben, PB = Peelrand Block, EL = Ems Low. Brown rectangle represents the Tilburg area.Experimental dataset on mechanical properties for the Volpriehausen Sandstones .....	21

Figure 9: Leak off pressure test (LOT) data from the onshore Netherlands (for location see Fig. 1). (A) Measured leak off pressures and hydrostatic gradient (1 bar/10 m) and lithostatic (2.2bars/10 m) gradients (source Van Wees et al., 2014) .....	22
Figure 10: Picture of the selected Volpriehausen sandstones and claystone core slabs (2 x 1m long) from the well WNN1-S2. Below are the sections from which experimental samples were cored. The black bar is the scale: 5 cm. ....	23
Figure 11: Pictures of the GDS-HPETAS (a) and the inner cell experimental set up (b) used at the iM4RockLab – TNO Utrecht. ....	25
Figure 12: Pictures of the tested samples before and after the experiment. Dimensions for the undeformed plugs are in Table 6 The blurry appearance .....	26
Figure 13: Mohr–Coulomb criterion in $\tau$ – $\sigma'$ space. Also shown is Mohr's circle corresponding to a critical stress state (left). Orientation of the failure plane relative to the largest principal stress (right). From Fjaer et al. (2008).....	27
Figure 14: Experimental procedure for ELFO_1a showing confining pressure, differential axial stress, pore pressure, temperature, axial strain, radial strain and bulk strain as a function of time. The experiment time series for all the experiments can be found in Appendix A. ....	28
Figure 15: Volumetric thermal expansion coefficient as a function of temperature. $P_e$ indicates the effective confining pressure of temperature increase. ....	29
Figure 16: Peak differential stress (a), angle of internal friction (b), cohesion (c), Young's modulus (d), Poisson's ratio (e) and volumetric thermal expansion coefficient (f) as a function of initial He porosity. ....	30
Figure 17: He porosity (a), Young's Modulus (b), Poisson's ratio (c), Peak differential stress (d), angle of internal friction (e), cohesion (f) and volumetric thermal expansion coefficient (g) as a function well depth. Red dots: studied samples, black dots: previous analyzes. Blue area: RBMVU, green area: RBMVC, red area: RBMVL. ....	31
Figure 18: Map of reference wells WED-03 and WVN-03 relative to Tilburg AOI (modified from Dalby 1998).....	32
Figure 19: Gamma ray logs for the selected wells in the sandstone rich zones, showing different zonations .....	33
Figure 20: NLOG ThermoGIS overview map of heat in place for the Netherlands (ThermoGIS 2022) 34	
Figure 21: Reservoir temperature map (base case) of the Upper Volpriehausen Sandstone (RBMVU) in Southern Netherlands, placemark on map indicates Tilburg project location .....	35
Figure 22: Raw geoscience data prior to completing 3D geological modelling workflow .....	36
Figure 23: Structure of the Top Lower German Triassic sandstone unit (green contoured) showing variable offsets of intersecting faults (colored polylines on structure) 1x VE. ....	37
Figure 24: Defined 100x100x25m grid cell size of the simulation grid depicting stair step fault geometry and true geological structure. ....	38
Figure 25: Scenario of Eavor-Loop placement following downdip structural plunge yields horizontal lateral lengths of 3,000m. This scenario requires land acquisition in a densely populated area and as a result is an unrealistic scenario. ....	39
Figure 26: Scenario of Eavor-Loop placement following updip structural climb yields horizontal lateral lengths of 2,100m. This scenario is preferred from a land acquisition standpoint as land is more readily available than in the city scenario. However, drilling updip horizontally is more challenging and results in shorter lateral lengths than the downdip scenario due to higher modelled torque and drag. ....	40
Figure 27: Amer heat network with the Tilburg Eavor-Loop location shown in orange circle .....	41
Figure 28: Project location and Amer heat network. ....	41
Figure 29: Subsurface laterals projected onto the surface. ....	42
Figure 30: Generic site layout during drilling operations with two drilling rigs.....	43
Figure 31: Layout of Eavor-Loop production facilities.....	44
Figure 32: Vertical to the horizontal well profile of the Tilburg stratigraphy VE = 1x .....	45

---

Figure 33: Lateral Eavor-Loop placement within the Lower German Triassic sandstone package. Structural maps depict the Base Volpriehausen sandstone structure. Colored surfaces indicate faults including two sub-seismic resolution lineations (yellow and blue) crossing the Eavor-Loop..... 46

Figure 34: Schematic of effective thermal radius vs. spacing between two horizontal laterals to avoid heat transfer interaction..... 49

Figure 35: Process flow diagram – summer operations ..... 51

# 1. General

## 1.1. Introduction

The goal of WP1 was to assess the feasibility of the use of Eavor-Loop technology for the extraction of geothermal heat to be used as a source for the Amer heat network. The work included a thorough geological and geomechanical interpretation of the subsurface, to assess the suitability of the geological conditions both from a drilling perspective and from a heat delivery point of view. In addition, the subsurface feasibility was evaluated in an economic context.

The first hurdles which apply to any geothermal development in the Netherlands were taken by selecting an area with available 3D seismic and a heat network with sufficient capacity for 100% utilization of a new geothermal heat source.

The 3D seismic survey was interpreted and depth corrected with standard geophysical interpretation tools. Faults and target formation tops were identified with little uncertainty. The available seismic survey unfortunately did not cover the full extent of the heat network, which limited the optimization of the placement of the loop, which was further exacerbated by the restrictions in suitable surface locations in this area. Eventually, one complete loop (12 laterals) was defined as a feasible scenario considering the limitations in the area. The lateral length is limited in this case due to the fact that from the selected location the laterals will have to be drilled updip in a Southward direction, following the dip of the target formation. Updip drilling limits the maximum length of the laterals due to drilling mechanics in this case to approximately 2000m to 2500m. Longer laterals would make the project more economical, however this location do not seem to be feasible.

Offset well data was investigated for the temperature gradient and the relevant formation properties of the target Triassic Bunter sandstone formation. The temperature gradient was confirmed to be better than expected at 35 °C/km. The conductivity of the Bunter has been measured as well as the unconfined compressive strength. The conductivity was also a bit better than expected and the formation strength is sufficient for the stability of the open-hole laterals throughout the productive life of the loop as shown by modelling of the near well bore stresses. The formation permeability is very low which is helpful for the Rock-Pipe™ sealing.

The drilling plan for the vertical wells was constructed based on offset well experience. Combining the knowledge of the wells drilled with the new requirements for geothermal wells resulted in a concept casing design and time and cost estimate. For the drilling of the laterals in the target Bunter formation the rate of penetration and the bit life were estimated by comparing rock hardness with the results from the hard rock drilling research at Utah Forge. The estimates were judged to be manageable.

The heat output was calculated with the Eavor heat flow and thermodynamic modelling. The current inlet temperature of the Amer heat network at 110 °C is quite high in the wintertime (95°C in the summer). This temperature is not often needed but the old network is not able to withstand quick temperature changes. This high inlet temperature is not good for the efficiency of the loop, as it requires a low circulation rate. This problem can be overcome by the use of a heat pump to boost the outlet temperature by taking more heat out of the return flow. The optimum capacity for a 30-year flat profile is modelled to be 9.1 MW in summer months and 7.1MW in winter months.

The economic feasibility is based on an estimated CAPEX of 54.5 MM € to construct the Tilburg Eavor-Loop, yielding an annual heat production of 74,000 MWh. OPEX is estimated at 162k €/year and the electricity demand of 660 kW to power an on-site heat pump to meet the heat network demand. The project is eligible for subsidized energy pricing through the SDE++ program.

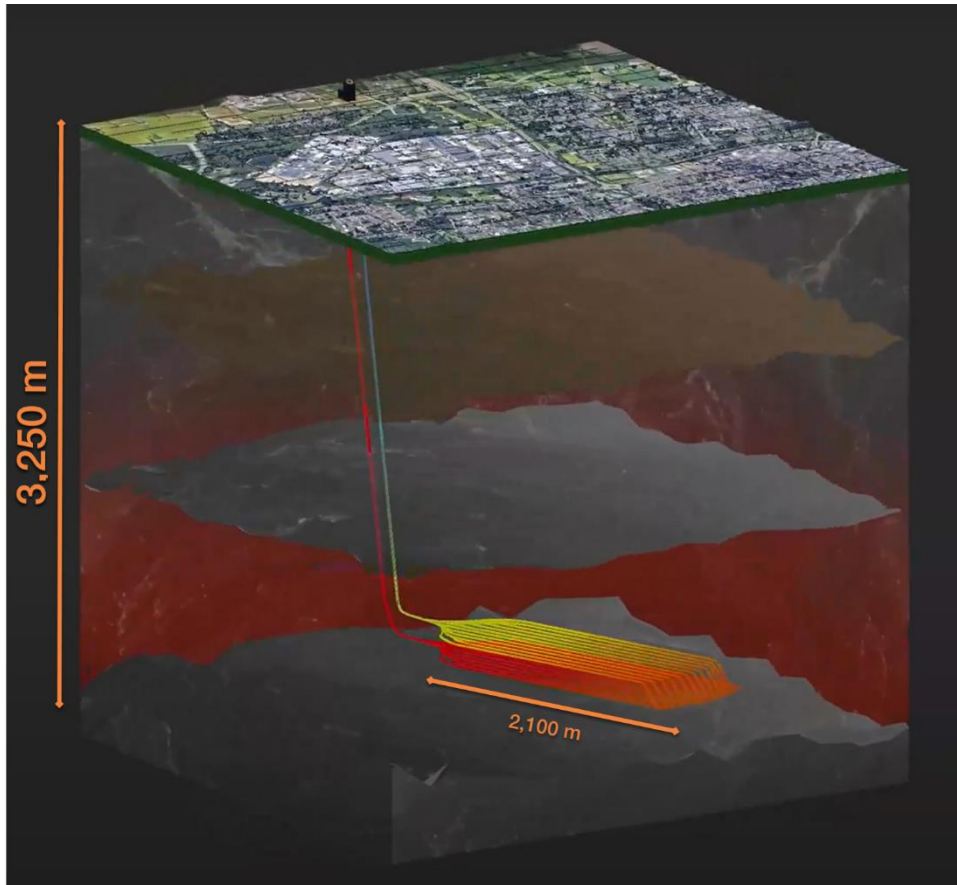


Figure 1: Stylized schematic of the Eavor-Loop planned near Tilburg

## 1.2. WP1 Goals & Objectives

In order to quantify suitable prospective conditions for Eavor-Loop development, a detailed characterization of the subsurface must be conducted. Geological and geophysical reservoir characterization is performed to provide inputs required for thermodynamic modelling and to de-risk the drilling execution and future operability of the Eavor-Loops, particularly in structured basins.

An interplay of geologic parameters forms the main drivers for maximizing the thermodynamic performance of Eavor-Loop projects. The relationship between thermal conductivity, porosity and temperature must be determined to create an accurate prediction of the thermodynamic performance of the Eavor-Loop system. Temperature can be directly acquired from downhole measurements and correlated to mapped geothermal gradients in the selected area. Thermal conductivity can be measured or calculated on direct rock samples and can be affected by porosity, mineralogy, and diagenesis. Finally, a detailed interpretation of the subsurface structures, lithologies and depositional setting can greatly improve the deliverability of multi-lateral drilling and aid in identifying drilling hazards. The goal of WP1 of the ELFO project is to identify and interpret the geological parameters and subsurface conditions and to evaluate the construction costs that support economic Eavor-Loop deployment

## 1.3. Data availability & uncertainty

The units used in this report relate to the International System of Units (abbreviated SI from the French *Système International*). All distances are expressed in metres or in kilometres. Temperatures are expressed in degrees Celsius. All coordinates are represented in the new Netherlands National

Triangulation System (*Rijksdriehoekstelsel*). Georeferenced data from different projection systems were converted to this system.

### 1.3.1. Well Data

Reference wells are listed in Table 1 and plotted in Figure 1. Wells were chosen based on proximity to the target area, data availability and quality, as well as reservoir characteristics.

The most relevant wells are HBV-01 and WWS-02, since they are the closest to the planned Eavor-Loop and are respectively located on the West and East structural highs bounding the target basin. No well penetrates the targeted basin, but the combination of well data and seismic quality is sufficient to guarantee an overall solid horizon interpretation and property forecast, even if with some degree of uncertainty.

Table 1: Selected wells for the study and the purpose for which well data were used.

Well	Year drilled	Well tie	QC Velocity model	Correlation	Notes
BKZ-01	1989			Yes	TD Rogenstein Mb
HBV-01	2002	Yes	Yes	Yes	TD Rogenstein Mb
HVB-01	1995			Yes	TD L. Volpriehausen Sst Mb
SMG-01	1969			Yes	TD L. Buntsandstein Fm
SPC-01	1987			Yes	TD Maurits Fm
SPG-01-S2	1994			Yes	TD U. Volpriehausen Sst Mb
STH-01	1987			Yes	TD Hellevoetsluis Fm
WWK-01	1987			Yes	TD Rogenstein Mb
WWN-01-S2	1989			Yes	TD Rogenstein Mb
WWN-03	1998			Yes	TD U. Volpriehausen Sst Mb
WWS-01-S1	1991		Yes		TD Rogenstein Mb
WWS-02	2005	Yes	Yes	Yes	TD Nederweert Sst Mb

All well data used in the study are publicly available, no confidential data were used.

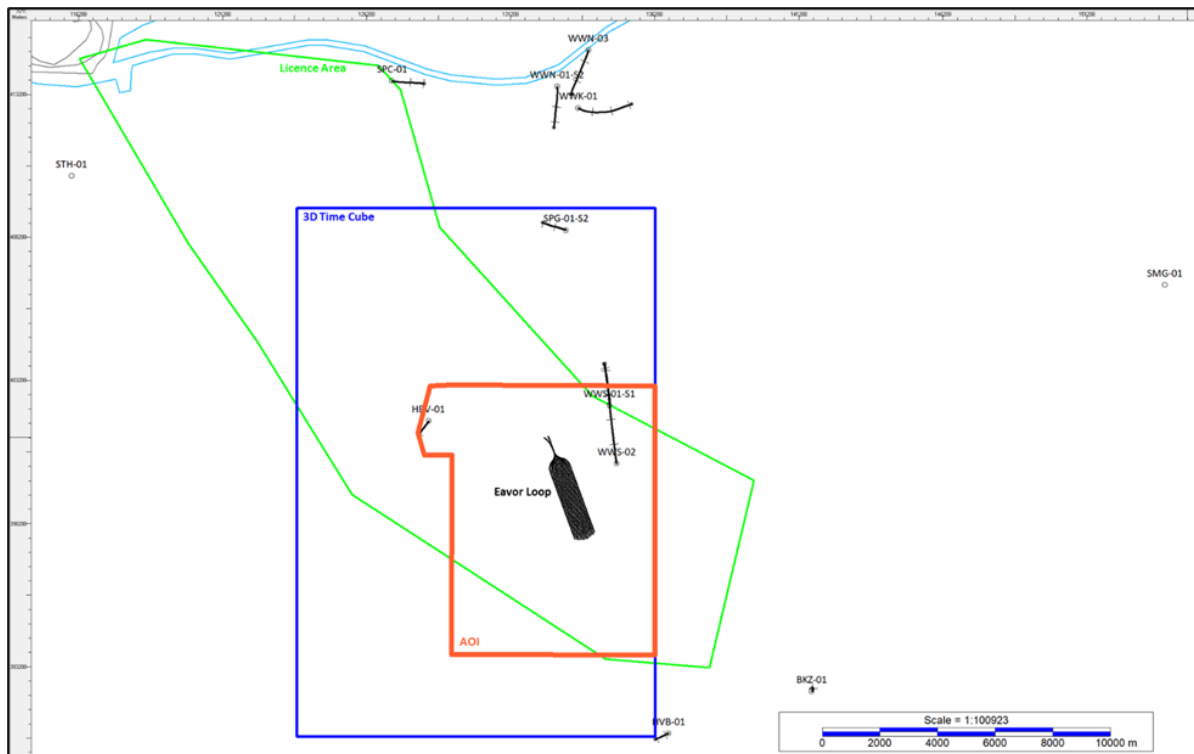


Figure 2: Location of wells and seismic data used in the study

### 1.3.2. Seismic Data

The Tilburg AOI is fully covered by a 3D seismic cube (Figure 2):

- L3CLY2001A (3D\_Tilbwaalw\_TWT): time cube of good quality

Seismic interpretation is entirely carried out on the above-mentioned cube.

The seismic survey is displayed as SEG normal polarity, meaning that all seismic sections shown in this report are displayed such that a positive number (black colour) represents a hard kick (an impedance increase). The geometry of the L3CLY2001A seismic survey is given in Figure 3.

Survey Details

All Surveys  Working Set

Survey List

Search:  Filter Reset

3D\_Tilbwaalw\_TWT  
 4213\_mig160001  
 4215\_mig160001  
 4231\_mig160001  
 4234\_mig160001  
 562\_mig160001  
 702001\_mig160001  
 702002\_mig160001  
 702003\_mig160001  
 702004\_mig160001  
 702005\_mig160001  
 702006\_mig160001  
 702014\_mig160001  
 702015\_mig160001  
 702016\_mig160001  
 702017\_mig160001

XY Units: Meters  
 Show XY Limits  
 Show Lat-Long Limits

X Coordinate Range:  
  
 to

Y Coordinate Range:  
  
 to

General Acquisition Processing

Survey Name:

Data Type: \*Amplitudes (Time)

Source of Data:

Processor:  New...

Date Loaded: (mm/dd/yyyy)   
 Date Processed: (mm/dd/yyyy)

Short Description of Processing:

Long Description of Processing (3200 characters)...

SEG Y Text Header (3200 characters)...

Time Range:  to  sec.

Datum Elevation:  Meters

Replacement Velocity:  Meters/sec.

Applications  
 Structure  
 Stratigraphy

Fold:

Record Length:  sec.

Samples Per Trace:

Sample Interval:  sec.

Storage Format:  bits

RMS:

Phase in Zone of Interest:  deg.

Average Frequency:  Hz

Bandwidth:  Hz

3D

	Min. Value	Max. Value	Increment	Spacing	Count
Inline:	<input type="text" value="8679"/>	<input type="text" value="9603"/>	<input type="text" value="1"/>	<input type="text" value="20"/>	<input type="text" value="925"/>
Crossline:	<input type="text" value="8019"/>	<input type="text" value="8641"/>	<input type="text" value="1"/>	<input type="text" value="20"/>	<input type="text" value="623"/>

OK Cancel Apply Help

Figure 3: Geometry of the L3CLY2001A survey (3D\_Tilbwaalw\_TWT).

## 2. WP1 Subsurface Feasibility

### 2.1. Seismic interpretation

#### 2.1.1. Method

The Eavor Geoscience team commissioned Panterra Geoconsultants B.V. to complete the seismic interpretation on the Tilburg L3CLY2001A (3D\_Tilbwaalw\_TWT).

Seismic interpretation and generation of depth and thickness maps were carried out in Kingdom 2019 as part of the Tilburg study. Horizons and faults were picked every 10<sup>th</sup> inline and crossline except for Base North Sea and Base Cretaceous horizons, obtained by converting TNO grids and refining them every 10<sup>th</sup> inline and crossline. Note that the AOI is fully located within the L3CLY2001A time cube.

#### 2.1.2. Well-to-Seismic Ties

The seismic interpretation was performed in the time domain only; therefore, a well-to-seismic tie was required to compare well and seismic data. However, no well provided with check-shots reached the target interval within the seismic cube area. For this reason, check-shots from well WWK-01 were used to derive interval velocities for the deeper stratigraphy of the AOI (from Rogenstein Member to Aalborg Formation), while a local seismic match was applied to shallower stratigraphy (from Werkendam to Ommelanden Formation), where check-shot points were not available or not representative for the AOI.

In general, there is good confidence in the seismic picks based on the well tie; the seismic character of the horizons (e.g., hard kick, soft kick, see Table 2) is in good agreement with the sonic logs of the wells.

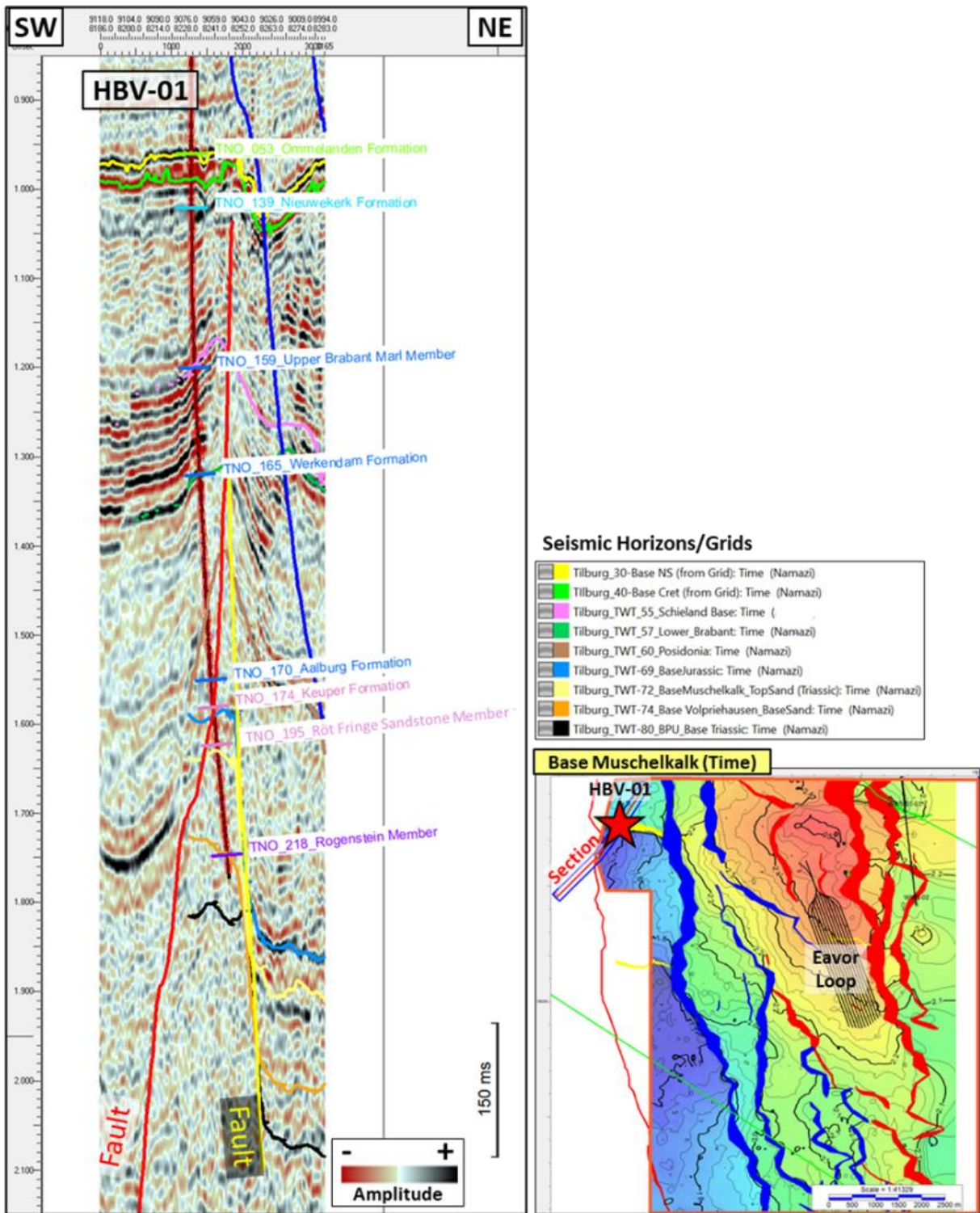


Figure 4: Seismic to well tie for HBV-01

### 2.1.3. Seismic Interpretation

As stated in Section 2.1.2 and listed in the table below, nine seismic horizons were interpreted on the available time cube.

Table 2: List of key horizons interpreted for this study and their character

Horizon	Well top name	Seismic character	Quality	Interpretation method
Base North Sea	TNO_053_Ommelanden Formation	Strong hard kick	Excellent	Grid based / Manual pick
Base Cretaceous	TNO_139_Nieuwekerk Formation	Strong soft kick	Excellent to good	Grid based / Manual pick
Base Schieland	TNO_159_Upper Brabant Marl Member	Strong hard kick	Good	Manual pick
Base Lower Brabant	TNO_165_Werkendam Formation	Strong hard kick	Good	Manual pick
Top Posidonia	TNO_170_Aalburg Formation	Strong hard kick	Good	Manual pick
Base Jurassic	TNO_174_Keuper Formation	Strong to moderate hard kick	Good to moderate	Manual pick
Base Muschelkalk	TNO_195_Röt Fringe Sandstone Member	Strong to moderate soft kick	Moderate	Manual pick
Base Volpriehausen	TNO_218_Rogenstein Member	Moderate hard kick	Moderate	Manual pick
Base Triassic	NA	Moderate hard kick	Moderate	Manual pick

All seismic sections shown in this report adhere to the seismic character given in Table 2. This means that positive seismic amplitudes representing a hard kick are black in color, e.g. Base North Sea pick.

The seismic character of the different stratigraphic intervals played an important role in ambiguous situations and when additional information was unavailable.

All horizons listed in Table 2 were interpreted on every 10th inline and crossline of the AOI. This resulted in a dense grid further used as input for creating time maps and thus avoids additional uncertainties from an unconstrained interpolation algorithm.

Faults were interpreted on every 10<sup>th</sup> inline and crossline of the AOI too. Results of the interpretation show a main NW-SE fault trend forming a graben structure, about 4 km wide at reservoir level (see Figure 5 and Figure 6). The graben is crossed by several minor faults, either parallel to the main trend or with a WNW-ESE trend linking the main faults in a pop-up (S of the AOI) to pull-apart fashion (N of the AOI). Fault density decreases from South (average fault spacing ~0.8 km) to North (average fault spacing ~1.5 km). The largest (~2 km wide) fault block is located in the middle of the AOI and represents the target of the Eavor-Loop.

#### 2.1.4. Gridding Algorithm

All horizons were gridded using the Flex Gridding algorithm and a cell size of 20 x 20 m. The resulting grids were additionally smoothed to a moderate degree. Fault polygons were generated automatically at first and then manually edited to improve the fit with grids.

#### 2.1.5. Time-Depth Conversion

A depth dependent linear velocity function is used to convert the time interpretations to depth. The  $V_0, k$  function applied describes the interval velocity as a function of depth,  $Z$ , and has the following form:

$$V_{int} = V_0 + k * Z \quad (1)$$

Vertical lithological changes are not modelled with this function and the  $V_0$  and  $k$  parameters describe the combined effects of burial and lateral lithological changes. The parameters used are based on the TNO Velmod-3.1 seismic velocity model (TNO, 2017). While the model assigns a fixed  $k$  value for each velocity layer,  $V_0$  is characterized by lateral variations. As a result, a representative  $V_0$  value was selected for the specific Tilburg target area, as determined from the regional  $V_0$  maps provided with Velmod-3.1.

In total, five velocity layers have been defined:

- North Sea Supergroup
- Cretaceous (Chalk group)
- Schieland (Upper Jurassic)
- Altena (Lower Jurassic, including Lower Brabant, Posidonia and Base Jurassic layers)
- Triassic (including Muschelkalk, Volprieausen and Base Triassic layers).

The  $V_0$  and  $k$  parameters for the best fit model for each layer are summarized in Table 3.

Residuals between well tops and time-depth converted grids show a good (<3%) to very good (<1%) fit in average. The single poorly correlated point (>5% residual) is found at the Base Volprieausen horizon in well WWS-01-S1. However, screening of the seismic cube along the well path shows that WWS-01-S1 reaches the Base Volprieausen in proximity (or even within) a fault zone. Therefore, the mismatch is likely a local issue only associated with the lateral uncertainty of the fault location. The very good fit of the shallower tops for the same well is further evidence of the quality of the time-depth conversion method at this location.

Depth differences and residuals are summarized in Table 4.

Table 3:  $V_0$  and  $k$  parameters used for the time depth conversion

Velocity layer	$V_0$ (m/s)	$k$ ( $s^{-1}$ )
North Sea	1850	0.284
Cretaceous	2400	0.889
Schieland	2300	0.52
Altena	2200	0.436
Triassic	3000	0.374

Table 4: Table showing the depths differences and residuals between wells and time-depth converted grids

Grid	HBV-01				WWS-02				WWS-01-S1				Average	
	Z Well	Z Grid	Residual (m)	Residual (%)	Z Well	Z Grid	Residual (m)	Residual (%)	Z Well	Z Grid	Residual (m)	Residual (%)	Residual (m)	Residual (%)
Base North Sea	939.49	950	-10.5	1.1	1125.06	1133	-7.9	0.7	1124.71	NA	NA	NA	-9.2	0.9
Base Cretaceous	1033.49	1000	33.5	3.3	1165.52	1175	-9.5	0.8	1165.05	NA	NA	NA	12.0	2.1
Base Schieland	1310.66	1301	9.7	0.7	1791.36	1793	-1.6	0.1	1707.86	NA	NA	NA	4.0	0.4
Base Lower Brabant	1495.78	1470	25.8	1.8	2046.52	2011	35.5	1.8	1968.56	1911	57.6	3.0	39.6	2.2
Top Posidonia	NA	1674	NA	NA	2268.94	2291	-22.1	1.0	2233.96	2250	-16.0	0.7	-19.1	0.8
Base Jurassic	1819.76	1865	-45.2	2.4	2572.27	2571	1.3	0.0	2586.66	2613	-26.3	1.0	-23.4	1.2
Base Muschelkalk	1895.31	1940	-44.7	2.3	2646.16	2698	-51.8	1.9	2668.17	2678	-9.8	0.4	-35.5	1.5
Base Volpriehausen	2151.1	2155	-3.9	0.2	2891.41	2869	22.4	0.8	2982.09	2797	185.1	6.6	67.9	2.5
Base Triassic	NA	NA	NA	NA	NA	NA	NA	NA	NA	NA	NA	NA	NA	NA

### 2.1.6. Depth Map of Top/Base Formation

The Top and Base reservoir depth maps are displayed in Figure 5 and Figure 6 . They show the maps for the Base Muschelkalk and Base Volpriehausen, respectively. The new Eavor-Loop is planned in a graben bounded by a series of NW-SE trending faults that are present in the study area. The target location of the planned Eavor-Loop is situated in the centre of the fault block and the laterals are oriented parallel to the local major fault trend, minimizing the risk of intercepting faults along the planned horizontal trajectories.

Note, that the occasionally irregular character of fault intersections was quality checked and corrected in section 2.6. Subsurface 3D Geological Model.

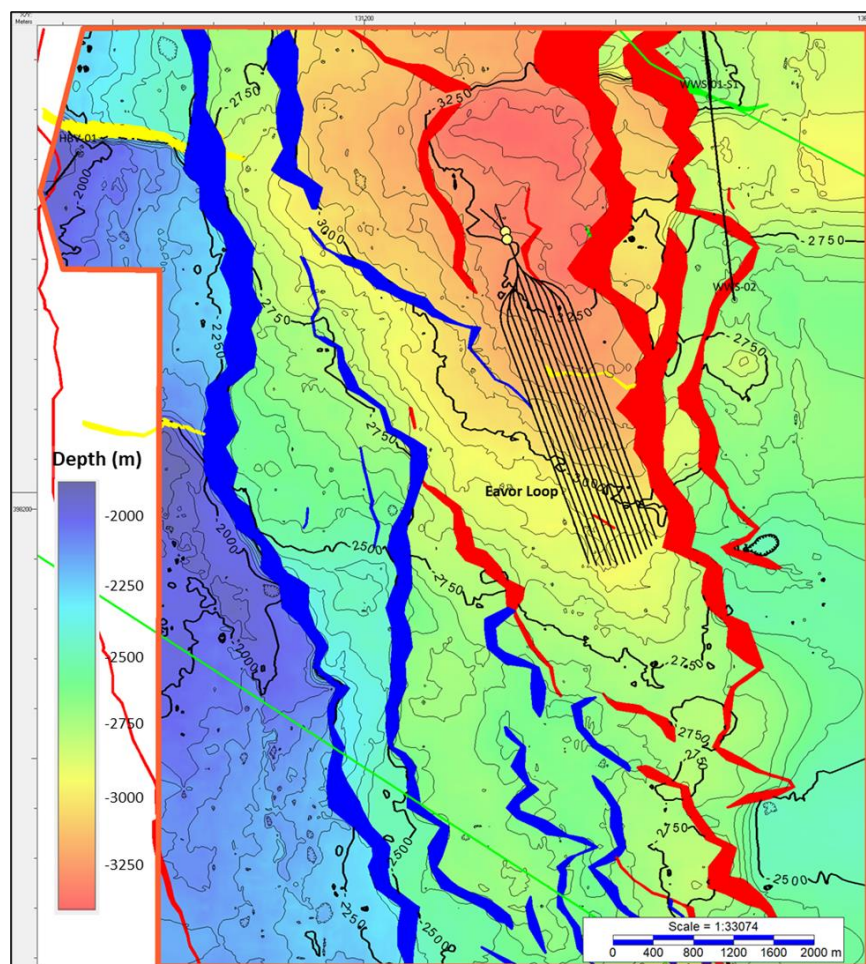


Figure 5: Base Muschelkalk (Top reservoir) depth structural map based on seismic interpretation (after time-depth conversion). Fault polygons in blue (E-dipping), red (W-dipping), yellow (N-dipping) and green (S-dipping). Orange polygon

shows Tilburg AOI, green lines show geothermal licence area. Yellow dots are Top reservoir penetration points. Contour interval is 50 m.

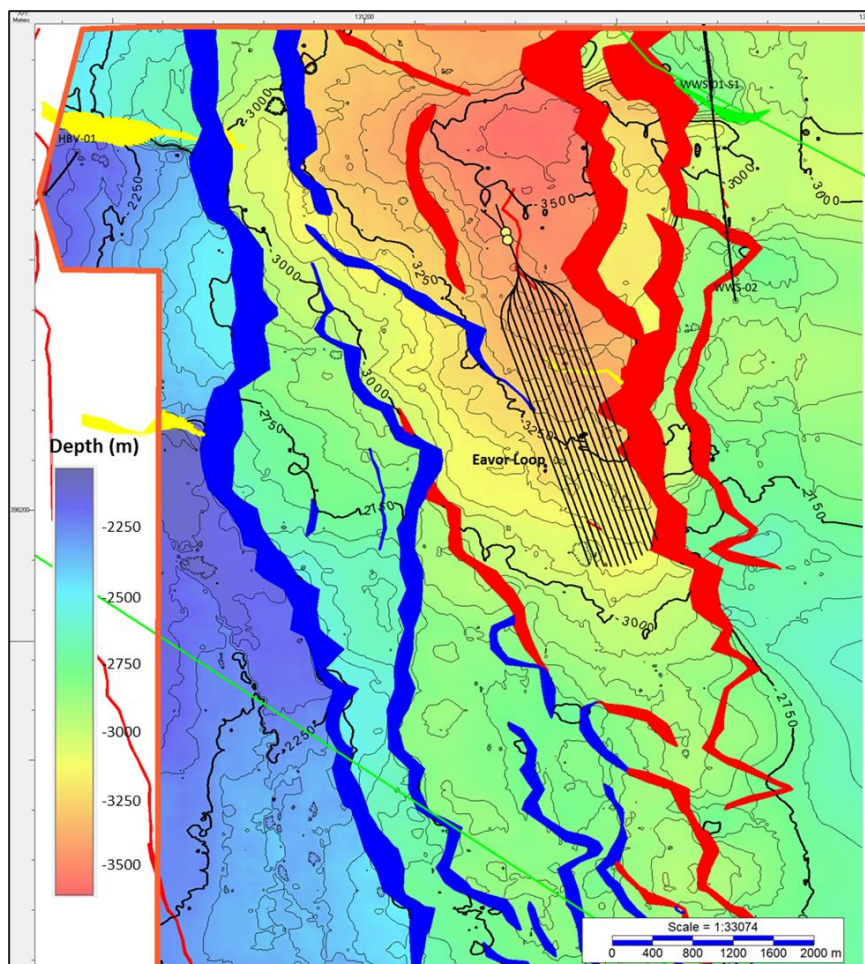


Figure 6: Base Volpriehausen (Base reservoir) depth structural map based on seismic interpretation (after time-depth conversion). Fault polygons in blue (E-dipping), red (W-dipping), yellow (N-dipping) and green (S-dipping). Orange polygon shows Tilburg AOI, green lines show geothermal license area. Yellow dots are Top Reservoir penetration points (base is not reached). Contour interval is 50m.

The reservoir thickness map was created by subtracting the depth-converted top and base interpretations (Figure 7). The map shows a relatively constant thickness of the reservoir, roughly around 150 m thick in most of the AOI, except for the northern part of the area, where the thickness in the graben tends to be above 200 m. Some local thickness variations are observed too, but they may be artifacts related to the local lower quality of the seismic data (e.g., the Easternmost part of the AOI, corresponding to the eastern edge of the seismic cube).

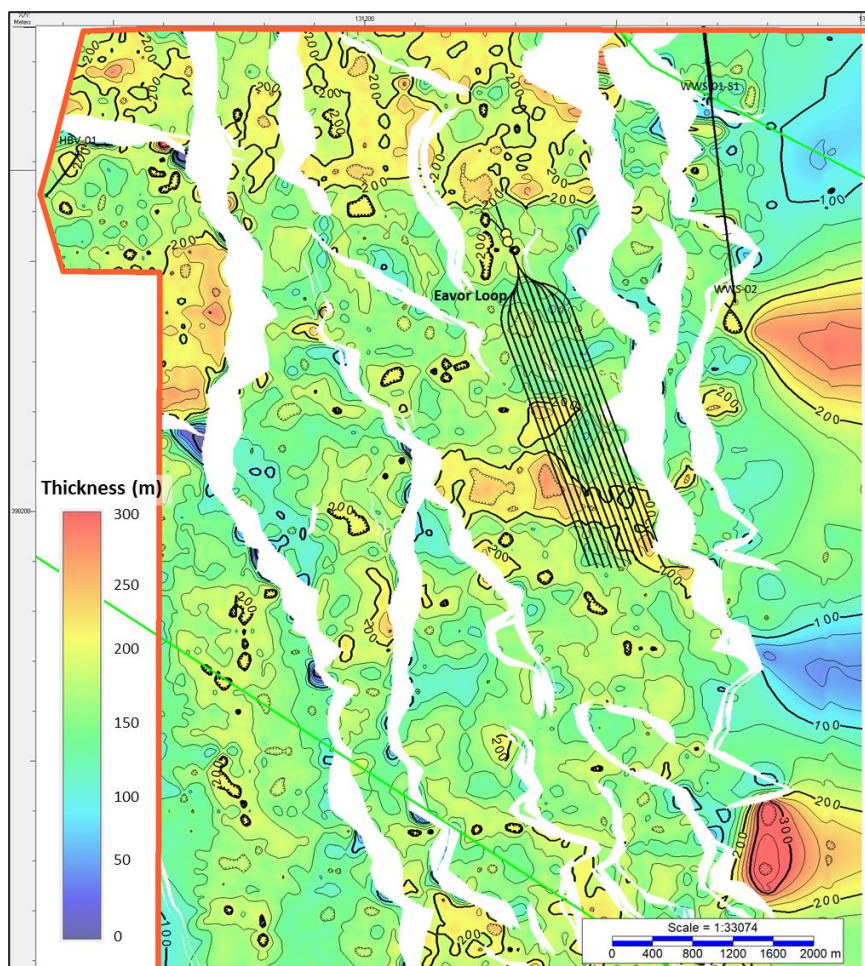


Figure 7: Thickness map of the reservoir (Triassic sandstone) based on seismic interpretation (after time-depth grid conversion). Orange polygon shows Tilburg AOI, green lines show geothermal license area. Yellow dots are Top reservoir penetration points (the base is not reached). Contour interval is 25 m.

The coordinates of the Eavor-Loop are listed in Table 5.

Table 5: Coordinates of Eavor-Loop surface location and targeted top reservoir

Well	Surface location		Top Reservoir		
	X (RD)	Y (RD)	X (RD)	Y (RD)	Depth (TVDSS)
Loop A1	132505.2	401253.5	132602.8	400976.2	-3292
Loop B1	132355.2	401203.5	132619.1	400898	-3265

#### 2.1.6.1. Discussion of Uncertainty of Top/Base Formation Map

The low residuals (see Table 4) give an overall good confidence in the accuracy of the depth maps. However, because no well has yet been drilled in the graben area targeted by the Eavor-Loop, some additional uncertainty needs to be taken into account. Based on the residuals table, this uncertainty should be <2% at the top reservoir level and <1% at the base reservoir level.

## 2.2. In-situ stress Tilburg area

### 2.2.1. Tectonic setting

National mapping programs and detailed structural analysis based on this data (TNO-NITG, 2004; Kombrink et al., 2012) provide an excellent structural characterization of the subsurface in terms of layering and faults. This mapping reveals a structure of Mesozoic and Cenozoic basin elements with sediment thickness of up to 5 km (Figure 8). The main tectonic events that affected the area were: (i) the Caledonian and Variscan orogenies, resulting in the assembly of the Pangea supercontinent during the Paleozoic, (ii) Mesozoic rifting, accompanying the break-up of Pangea, (iii) Alpine inversion, resulting from the collision of Africa and Europe during the Late Cretaceous and Early Tertiary, and (iv) Oligocene to recent development of the Rhine Graben rift system (Wong et al., 2007; Smit et al., 2020). These events have been marked by different stress fields, which repeatedly reactivated the existing faults, which were formed prior to the Mesozoic. The general structural model is, therefore, one of repeated (oblique) reactivation of basement faults which continue to control the structural grain, despite changes in tectonic regime and stress direction marked by extensional, transtensional and transpressional fault reactivation patterns; (Figure 8). Most faults dip at angles in excess of 60° or more. Crustal scale NW–SE oriented faults bounding basement elements such as the basin border faults in Figure 8 accommodate significantly more deformation than others, which may indicate a relative weakness deep in the crust compared to intact rock and smaller scale fault structures (Dirkzwager et al., 2000; Van Wees and Beekman, 2000).

### 2.2.2. In-situ stress South (East) Netherlands

In situ stress state in the Southern Netherlands World Stress Map data indicate that the stress pattern of north-western Europe is presently characterized by an overall NW–SE orientation of the maximum horizontal stress  $s_H$ , controlled by ridge push forces from the Mid-Atlantic Ridge and the collision of Africa and Europe (Grünthal and Stromeyer, 1992; Gölke & Coblenz, 1996; Heidbach et al., 2016; Plenefisch and Bonjer, 1997). The crustal stresses are sufficiently large in the south-eastern part of the Netherlands to cause significant neo-tectonic extensional deformation as reflected by differentiated Quaternary subsidence of the Roer Valley Graben and associated faulting (Cloetingh et al., 2010; Dirkzwager et al., 2000). The Roer Valley Graben (RVG) of the southeastern Netherlands, is the locus of the highest level of observed seismicity (Figure 8) in the Lower Rhine Graben (LRG), which forms the northeastern branch of the European Central Rift System, including the Rhine Graben toward the south (Cloetingh et al., 2010). The largest recorded earthquake in the LRG took place near Roermond 13-4-1992. It had a local magnitude of 5.8 and a moment magnitude of 5.4 (Camelbeeck, 1994). By inverting the focal mechanism data of the 1992 Roermond earthquake and its aftershocks it was found that the LRG is marked by normal faulting stress regime, for which the vertical stress is larger than the minimum and maximum horizontal stresses  $s_h$  and  $s_H$ , respectively and  $s_H$  orientation is N139° (Camelbeeck, 1994; Camelbeeck & Van Eck, 1994). The confidence interval of the stress inversion on the other hand suggests that N135–165 orientations are also possible. The estimated  $s_H$  orientation fits rather well to neo-tectonically active faults when projected to the surface, according to a fault dip of 60°. The critical ratio of shear and effective normal stress on these active faults (Worum et al., 2004) is expected to be close to the coefficient of friction to generate slip, which under the Mohr–Coulomb failure criterion is typically around 0.6 (Zoback & Townend, 2001). (Worum et al., 2004) analyzed through a slip tendency prediction for hypothetical orientation of  $s_h$  and different magnitudes of  $s_h$  and  $s_H$  relative to vertical stress  $s_v$ , which stress orientation and magnitudes give the best fit to the observed active faults. In line with findings from the focal mechanisms, it was concluded that the maximum principal stress of the stress field in the LRG is more likely vertical (normal faulting regime) than horizontal. In terms of stress orientation. Worum et al. found that the N145E orientation of  $s_H$

in the LRG results in slightly higher slip tendency values than a N160E orientation, favoring the first scenario.

In summary the in-situ stress state in the south-east Netherlands favors normal faulting with  $s_v > s_H$ , with a  $s_H$  orientation of 145–160°. The  $s_v$  magnitude increases with burial depth, which is estimated for the sedimentary infill in the Netherlands at 2.2 bars/10 m (e.g., Hofstee et al., 2009), but may increase at larger depth due to mechanical compaction (Bakx et al., 2022).

In the southwestern part of the Netherlands in the West Netherlands Basin, the minimum LOP pressures are estimated around 1.4 bar/m (Van Wees et al., 2014; Bakx et al., 2022) for depths up to 2500m, indicative for a minimum horizontal stress which is relatively close to conditions for active faulting observed in the RVG (Van Wees et al., 2014). For other areas in the Netherlands and for deeper burial conditions the LOP gradient is higher, indicative of a more stable stress field (Bakx et al., 2022).

### 2.2.3. Implications for the Tilburg area

The Tilburg area is located at the crossroads of the Roer Valley Graben and the West Netherlands (Figure 8). It is likely marked by an in-situ stress field with the orientation of maximum horizontal stress in direction with a  $s_H$  orientation of 145–160°, and a minimum  $s_H$  (LOP) in the range of 1.4 bar/10cm (see Figure 9).

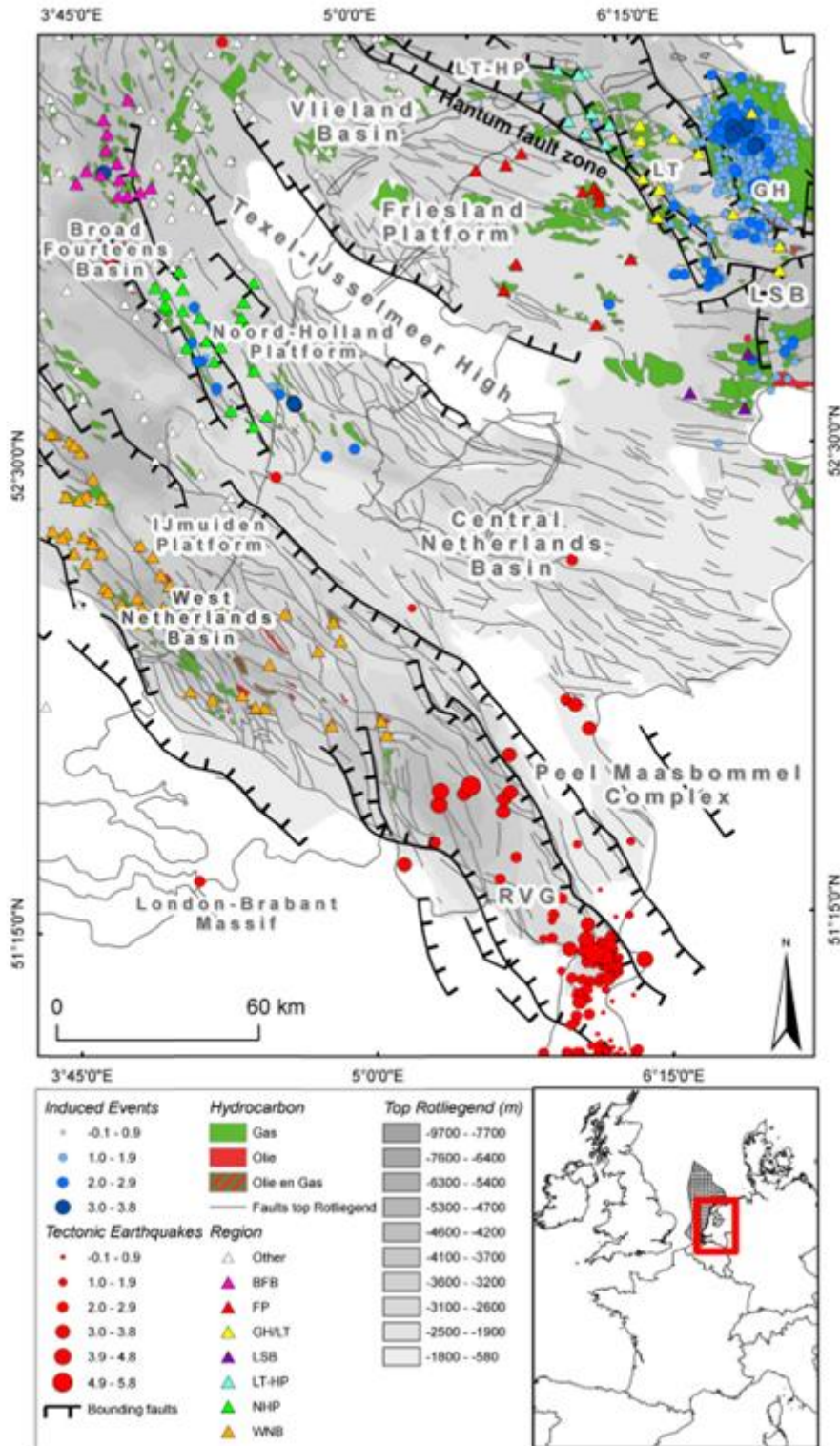


Figure 8: Overview of tectonic elements, seismicity and hydrocarbon reservoirs in the Netherlands (source Van Wees et al., 2014). Natural seismicity is shown in red circles, induced seismicity is shown in blue circles (larger events in yellow). Hydrocarbon reservoirs are indicated in green (gas) and red (oil). Major fault zones (solid lines) separate the main tectonic elements which characterize the subsurface of the Netherlands (after Wong et al., 2007). Triangles correspond to Leak off test (LOT). Colors denote different regions: BFB = Broad Fourteen Basin, FP = Friesland Platform, GH/LT = Groningen High/Lauwerszee Trough, LSB = Lower Saxony Basin, LT-HP = Lauwerszee trough-Hantum Platform, NHP = Noord Holland Platform, WNB = West Netherlands Basin. RVG = Roer Valley Graben, PB = Peelrand Block, EL = Ems Low. Brown rectangle represents the Tilburg area. Experimental dataset on mechanical properties for the Volpriehausen Sandstones

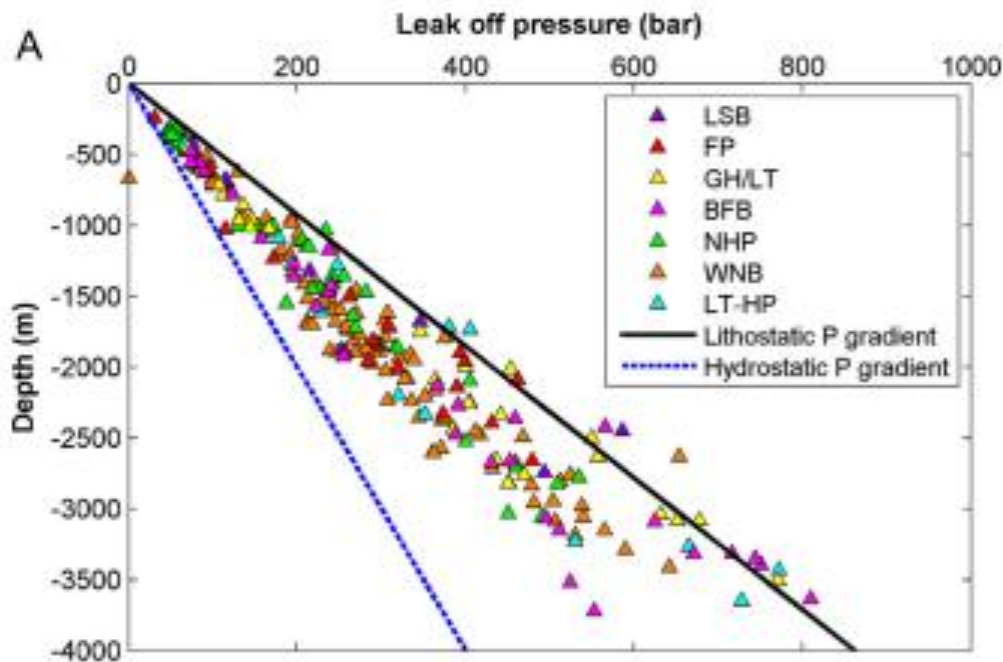


Figure 9: Leak off pressure test (LOT) data from the onshore Netherlands (for location see Fig. 1). (A) Measured leak off pressures and hydrostatic gradient (1 bar/10 m) and lithostatic (2.2bars/10 m) gradients (source Van Wees et al., 2014)

## 2.3. Experimental dataset on mechanical properties of the Volpriehausen Sandstones

The feasibility of the Eavor-Loop in the Tilburg area relies on the integrity of the borehole submitted to thermoelastic stressing, which corresponds to the change in stresses due to temperature variations. The modelling of the borehole integrity study is done in WP3, where more details on the physical mechanism governing thermoelastic stressing and its effect on borehole stability are given. To summarize, during thermoelastic stressing, the stress variation is proportional to the rock linear thermal expansion coefficient ( $\alpha$ ), young's modulus ( $E$ ) and Poisson's ratio ( $\nu$ ). The higher these parameters, the higher the stress. The failure potential resulting from the stress changes can be quantified by the Shear Capacity Utilization ( $SCU < 1$ : no shear,  $SCU = 1$ : onset of shear failure), which is inversely proportional to the Mohr-Coulomb criterion parameters: the cohesion, and the angle of internal friction. The higher these parameters are the less likely the borehole host rock is likely to fail.

In this chapter, we will describe and present the result from the experimental determination of the thermal expansion coefficient, elastic moduli, and Mohr-Coulomb criterion of the formation targeted by the Eavor-Loop in the Tilburg area.

### 2.3.1. Sample selection

The Volpriehausen sandstones (RBMV) are the formation targeted by the Eavor-Loop in the Tilburg area. To build accurate feasibility studies, determination of mechanical and thermomechanical parameters at stresses, pressures, and temperatures of the targeted formation.

Available cores sampling the RBMV in the Tilburg region geographically close and tectonically related to the targeted area were found in the well Waalwijk Noord-01-Sidetrack2 (WWN-01-S2). The well is

located 1,500 m West North of the Eavor-Loop placement in the footwall of a major normal fault of the RVB. The top and bottom of the RBMV appear at 2843 and 2969m TVD and therefore about 300m shallower than the targeted RBMV in the AOI. For this study, we assumed that, at such depth, the variations in mechanical properties related to different burial histories of the sediments (Vucelic et al. 2017) are negligible compared to the variations induced by porosity changes (Carcione & Cavallini 2002; Carcione et al. 2005; Heap et al. 2019; Wang 1984). We therefore considered that the RBMV samples from WWN1-S2 make a good analogue for the Volpriehausen formation in the AOI for the Eavor-Loop in the Tilburg area.

The cored samples from WWN1-S2 were available at the TNO, GDN, and Central Core Sample Storage at Zeist. The Upper Volpriehausen (RBMVU, Figure 10: ELFO\_1 and 2) are fluvial and aeolian light-brown and carbonate-cemented sandstones show an alternation of thin sandstone and greenish claystone laminae and the Lower Volpriehausen (RBMVL, Figure 10: ELFO\_4 and 5) is a well-defined pink to grey fluvial arkosic sandstone (Ames and Farfan, 1996). They are separated by the Volpriehausen clay-siltstone member (RBMVC, Figure 10: ELFO\_3) composed of red or green cycles of fine-grained sandstone, siltstone, and claystone with sometimes intercalated Oolite beds (van Adrichem Boogaert and Kouwe, 1994). Core analyses (porosity, permeability, grain density) were available on RBMV samples up to 2921m TVD (<https://www.nlog.nl/datacenter/brh-overview>). The porosity of the Volpriehausen sandstone is highly variable from 3 to 11% and decreases with depth (Figure 17). Our sampling strategy was based on selecting porosity endmembers for RBMVU and RBMVL as well as testing RBMVC. Based on the available porosity measurement, sections of the core were selected however we observed that the porosity was highly variable at a small scale, nonetheless we were able to sample a wide range of porosity (4.1 - 9.8 %). All selected sandstones were tested but unfortunately it was not possible to extract intact cores from the claystone ELFO\_3. The important mechanical and thermomechanical parameters for the tested samples are shown in Table 6.

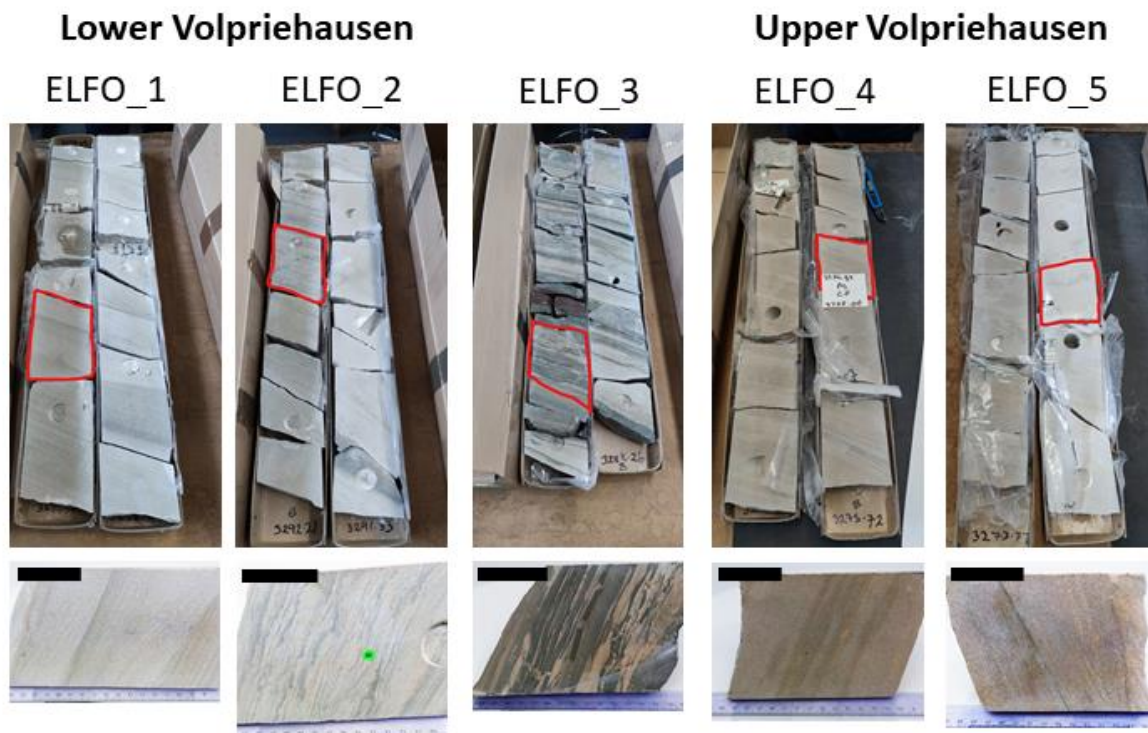


Figure 10: Picture of the selected Volpriehausen sandstones and claystone core slabs (2 x 1m long) from the well WNN1-S2. Below are the sections from which experimental samples were cored. The black bar is the scale: 5 cm.

### 2.3.1.1. Experimental setup

All experiments and measurements of static elastic parameters were performed in the iM4RockLab of TNO Applied Geosciences in Utrecht. The experiments were performed with a High Pressure Environmental Triaxial Automated System from GDS instrument (GDS–HPETAS, Figure 11a). This apparatus can be operated at maximum confining and pore pressures of 65 MPa, can apply a maximum axial load of 250 kN and temperatures up to 100 °C. To measure the sample axial and radial deformation, local linear variable differential transformers (LVDT) were used: 2 axial LVDTs to measure the axial strain and 2 radial LVDTs to measure the radial strain (Figure 11b). Before the experiments, the local LVDTs were calibrated at temperatures and pressures relevant to our experiments' conditions. All parameters were recorded at a sampling rate of 1 Hz.

Table 6: Experiments summary

Parameters	ELFO_1a	ELFO_1b	ELFO_2b	ELFO_4a	ELFO_5
Formation	RMBV_L	RMBV_L	RMBV_L	RMBV_U	RMBV_U
Lithology	Sandstone	Sandstone	Sandstone	Sandstone	Sandstone
Well depths (m)	3298.49-3299.38	3298.49-3299.38	3291.33-3292.21	3274.81-3275.72	3271.97-3272.16
TVD (m)	2915.06-2915.92	2915.06-2915.92	2908.17-2909.02	2892.27-2893.15	2889.54-2889.72
Length (mm)	52.645 ± 0.047	54.115 ± 0.013	50.392 ± 0.053	50.392 ± 0.053	44.08 ± 0.156
Diameter (mm)	25.328 ± 0.039	25.345 ± 0.020	25.290 ± 0.046	25.290 ± 0.046	25.365 ± 0.015
He Porosity (%)	7.18	7.18	4.1	9.8	8.32
Lab Porosity (%)	6.14	6.66	5.0	6.3	5.5
Density matrix	2.63	2.63	2.69	2.68	2.70
Density saturated	2.52	2.52	2.60	2.48	2.49
In-situ Pe (MPa)	28	28	27.7	27.5	27
In-situ T (°C)	80	80	80	80	80
Peak stress (MPa)	221	212	194	191	-
Cohesion S <sub>0</sub> (MPa)	34 ± 6	26 ± 4	33 ± 4	41 ± 2	-
Internal friction Angle φ (°)	37 ± 3	40 ± 2	34 ± 2	29 ± 1	-
E <sub>s</sub> , Pe=1 MPa (GPa)	12.38 ± 1.10	7.28 ± 0.61	12.45 ± 0.60	10.04 ± 1.21	10.59 ± 0.84
E <sub>s</sub> in-situ P,T (GPa)	25.21 ± 1.12	23.12 ± 0.25	22.10 ± 0.52	21.64 ± 0.71	22.72 ± 0.71**
v <sub>s</sub> at Pe = 1 MPa	0.13 ± 0.01	0.29 ± 0.05	0.17 ± 0.02	-	0.26 ± 0.03
v <sub>s</sub> in-situ P,T	0.12 ± 0.01	0.05 ± 0.01	0.16 ± 0.01	0.14 ± 0.1	0.16 ± 0.04**
β (x 10 <sup>-5</sup> /°C)	2.65 ± 0.37	3.47 ± 0.25	1.80 ± 0.14	6.28 ± 0.39*	4.25 ± 0.23

± error: propagated from standard deviations and device accuracy.

\* Measured at Pe = 1 MPa

\*\* Measured at Room temperature

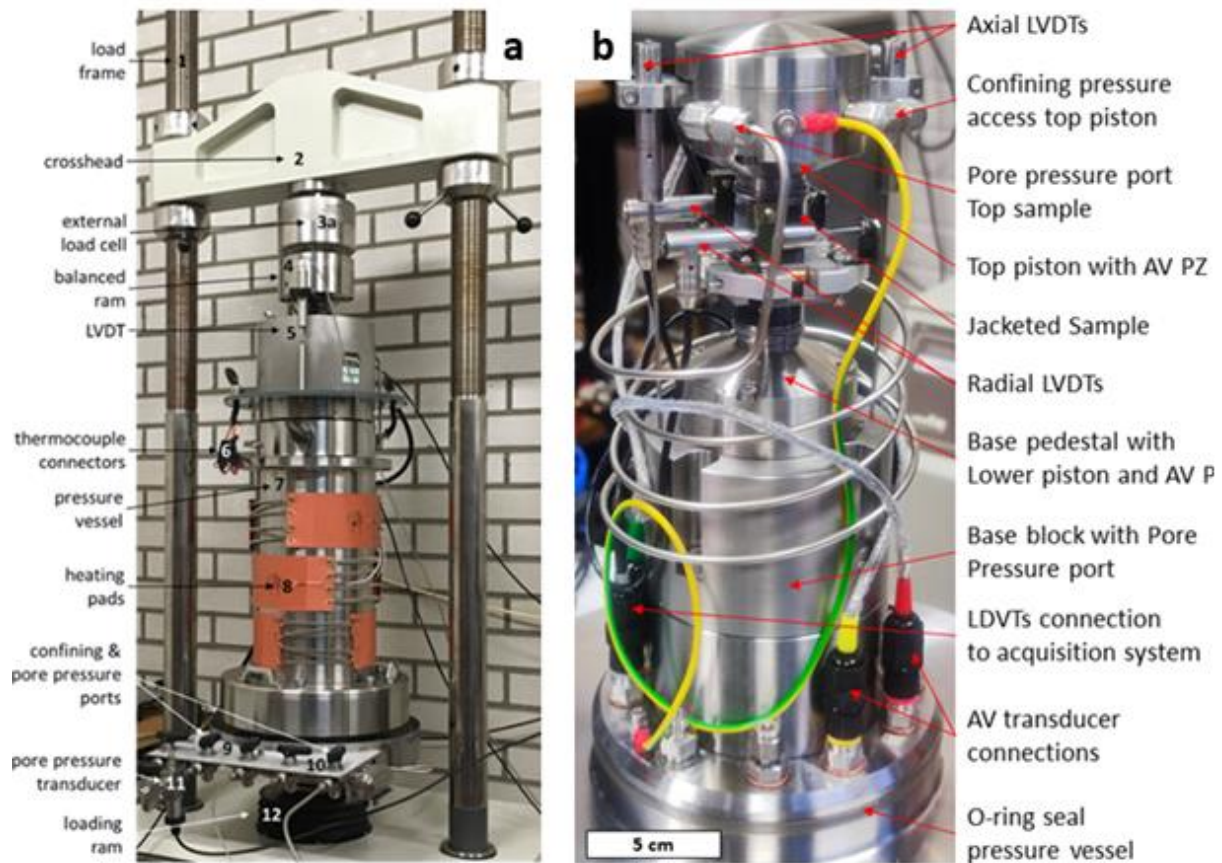


Figure 11: Pictures of the GDS-HPETAS (a) and the inner cell experimental set up (b) used at the iM4RockLab – TNO Utrecht.

The tested sample consists of a dry cylindrical core plug of 25 mm diameter and 44 to 54 mm length (Table 6, Figure 11). Before the experiments, the sample's weight is measured in dry, and water saturated (under vacuum) conditions to determine its density and porosity. The samples are placed in between the lower and upper piston within an FEP shrink tube isolating it from the confining oil. The sealing of the FEP tube is ensured by vacuuming the sample from the pore fluid drainage system for a few hours and tightening the jacket on the piston using a metal wire tourniquet (Figure 10b). The specimen is then saturated by flowing brine through for at least 12h. The brine was simulated using a saline solution with a salinity of 44700 ppm back calculated from resistivity logs from Röt and Detfurth sandstones. This salinity represents a lower limit for brines in these reservoirs as its low value results from water contamination during coring. During the experiment, pore pressure is controlled through the upper and lower pore fluid ports. To avoid issues with variability in samples in comparing data, it was chosen to determine many parameters and their relationship with effective confining pressure conditions and temperature on individual samples, rather than limiting duration of individual experiments by testing samples at a limited range of conditions.

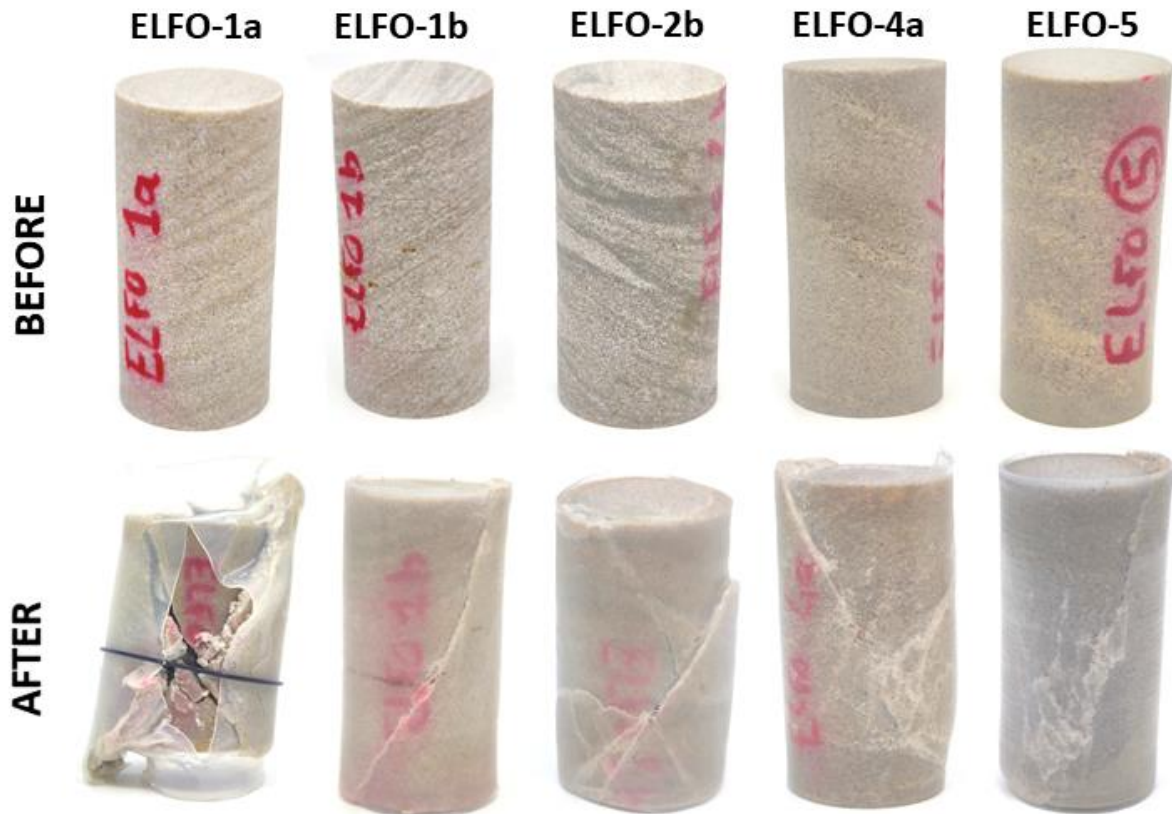


Figure 12: Pictures of the tested samples before and after the experiment. Dimensions for the undeformed plugs are in Table 6 The blurry appearance

### 2.3.1.2. Measurements of mechanical parameters and thermal expansion coefficient

The static elastic moduli represent the elastic behavior of a material undergoing large deformation in drained conditions and are therefore measured during the triaxial stages. The static elastic moduli we measured were Young's modulus  $E_s$  and Poisson's ratio  $\nu_s$ .

In a triaxial experiment, Young's modulus quantifies the elastic axial deformation of the material when a tensile or compressive stress is applied to it and is defined by the relationship:

$$E_s = \frac{\sigma_a}{\varepsilon_a}$$

Where  $\sigma_a$  is the axial differential stress, which is obtained by the ratio of the axial load of the surface area of the cylinder subtracted by the confining pressure, and  $\varepsilon_a$  is the axial strain recorded by the two axial LVDTs.

The Poisson's ratio quantifies the deformation of material perpendicular to the direction of the axial load and can be calculated from the following relationship:

$$\nu_s = -\frac{d\varepsilon_r}{d\varepsilon_a}$$

Where  $\varepsilon_r$  is the radial strain measured from the two radial LVDTs, both  $E$  and  $\nu$  were calculated during loading taking the slope between 57 and 77% of the maximum applied differential stress.

The coefficient of volumetric thermal expansion quantifies the change in volume of a body due to a change of temperature at a constant effective confining stress:

$$\beta = -\frac{d\varepsilon_b}{dT}$$

With T as the temperature. In literature, numerous studies refer to the linear coefficient of thermal expansion  $\alpha$  which is a third of  $\beta$  assuming a thermally isotropic material. In Earth Science, compression (stress) and contraction (strain) are positive, therefore  $\beta$  should be negative, however, in the literature  $\beta$  is always given as a positive value we therefore added a minus in front of the expression.

The Mohr-Coulomb criterion in 2 dimensions and this suitable for axial compression tests are defined by the linear relationship:

$$\tau = S_0 + \sigma' \tan \varphi$$

Where  $\tau$  is the shear stress,  $\sigma'$  the normal effective stress,  $S_0$  is the cohesion and  $\varphi$  the angle of internal friction. Figure 13 shows a Mohr-Coulomb criterion and Mohr's circle that touches the failure line. In that critical state, the failure plane will develop at an angle  $\beta$  from  $\sigma_3$  the principal direction of minimum stress. In our experiments, the Mohr-Coulomb criterion parameters  $S_0$  and  $\varphi$  were calculated by measuring  $\beta$  on the recovered samples and taking the peak axial effective stress  $\sigma_1'$  and effective confining stress  $\sigma_3'$  using the following relationships:

$$\varphi = 2\beta - \frac{\pi}{2}$$

and

$$S_0 = \tan \varphi \left( \frac{1}{\sin \varphi} \frac{\sigma_1' - \sigma_3'}{2} - \frac{\sigma_1' + \sigma_3'}{2} \right)$$

With  $\sigma_1'$  and  $\sigma_3'$  as maximum and minimum principal effective stresses correspond to the effective axial stress and effective confining pressure, respectively, in our experiments.

The ideal method would be to build the failure envelope based on several failure experiments on the same material at various confining pressures. However, due to the small number of available samples we opted for direct method where  $\beta$  was measured. As  $\beta$  is determined on recovered samples and because the fracture does not occur along a perfect plane (Figure 12), the uncertainty on the measurement and the calculated parameters are high but well in the expected range for sandstones (Table 6).

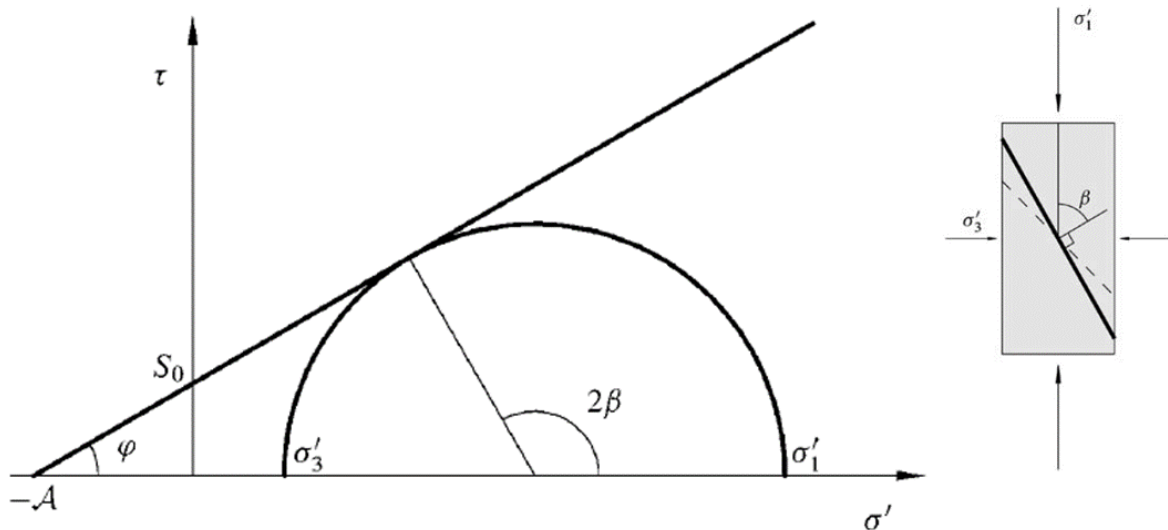


Figure 13: Mohr-Coulomb criterion in  $\tau$ - $\sigma'$  space. Also shown is Mohr's circle corresponding to a critical stress state (left). Orientation of the failure plane relative to the largest principal stress (right). From Fjaer et al. (2008).

### 2.3.1.3. Experimental procedure:

The experiments were designed to meet the standards from ASTM D 7012-14 (2014). Figure 14 illustrates the experimental procedure that was chosen for this project. The measurements were all done under drained conditions, i.e. at constant pore pressure meaning the pore fluid is free to circulate in and out of the sample to accommodate any change in pore volume resulting from any deformation. The “initial” conditions were set at 22°C and confining and pore pressure of 2 MPa and 1MPa, respectively, resulting in an initial effective confining pressure ( $P_e$ ) of 1 MPa. 3 triaxial tests were done at these conditions to measure the elastic parameters  $E$  and  $\nu$ , and then the confining pressure was raised to reach the effective mean stress assumed for the targeted reservoir. The mean effective stress is estimated using stress gradients for  $s_v$  of 2.2 bars/10m,  $s_{hmin}$  of 1.7 bars/10m (LOP at approximately 3000m depth) and hydrostatic pressure of 1 bar/10m which yields values of 27-28 MPa. It is important to note that if we have used a  $s_{hmin}$  gradient of 1.4 bars/10m we would obtain mean effective stresses of 34-35 MPa which would be an overestimation considering that  $s_{hmax}$ , which is not known, is not used for that calculation. 3 triaxial tests were then made at these conditions and then the temperature was raised to 80 °C, which corresponds to the measured temperature at the samples’ depths withing WVN1-S2. During this step, the volumetric thermal expansion  $\beta$  at reservoir stress condition was measured. Finally, 3 triaxial tests and a failure test were carried out at these conditions to obtain all the mechanical parameters at reservoir conditions.

The experiment ELFO\_5a failed at approximately 60 °C while raising the temperature (Appendix A), parameters given in Table 6 are therefore the one measure at reservoir stress conditions, but room temperature and the volumetric thermal expansion was measured only up to 60 °C.

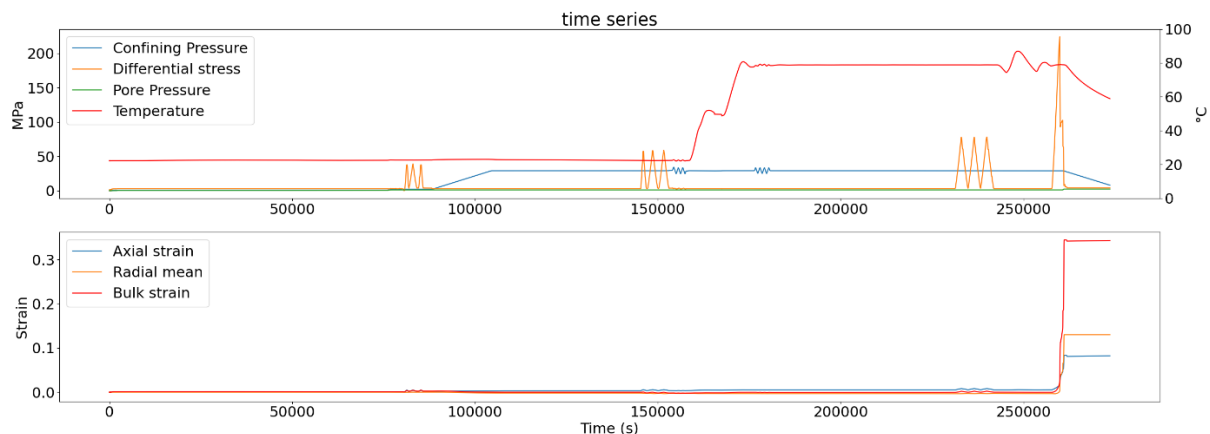


Figure 14: Experimental procedure for ELFO\_1a showing confining pressure, differential axial stress, pore pressure, temperature, axial strain, radial strain and bulk strain as a function of time. The experiment time series for all the experiments can be found in Appendix A.

### 2.3.1.4. Experimental results

The main results from our experiments are given in Table 6 and all measured parameters are given in Appendix B. Although most samples display the expected increase of volumetric thermal expansion coefficient  $\beta$  with increasing temperature (Figure 16), we have decided to average  $\beta$  over the low range of tested temperatures (22-80 °C) as a final value as the variation of  $\beta$  are small. It is important to note that the high  $\beta$  observed for ELFO\_4b is due to the low confining pressure (Somerton 1992).

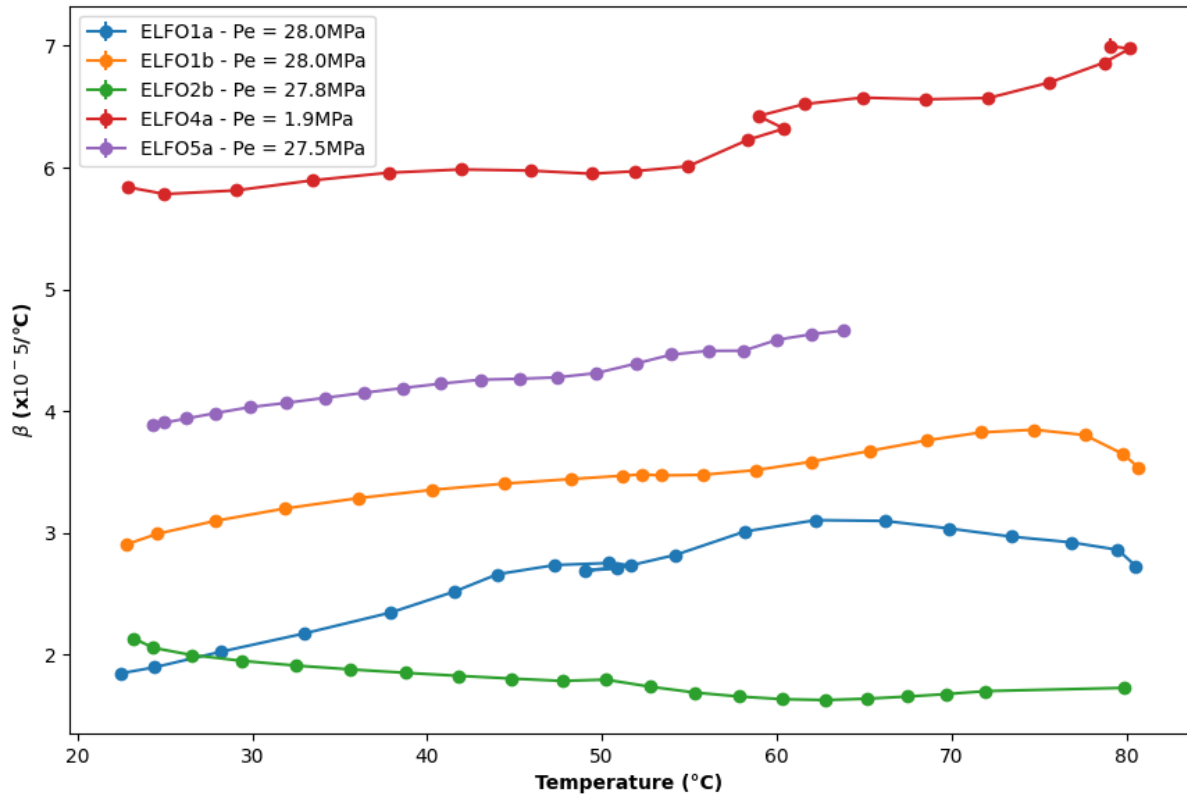


Figure 15: Volumetric thermal expansion coefficient as a function of temperature.  $P_e$  indicates the effective confining pressure of temperature increase.

The mechanical and thermomechanical parameters at reservoir P, T conditions are presented first against porosity (Figure 17) as it is considered a dominant factor for sandstone thermomechanical properties (Carcione & Cavallini 2002; Carcione et al. 2005; Heap et al. 2019; Wang 1984) and second against depth (Figure 18) to investigate any influence of burial history and lithology.

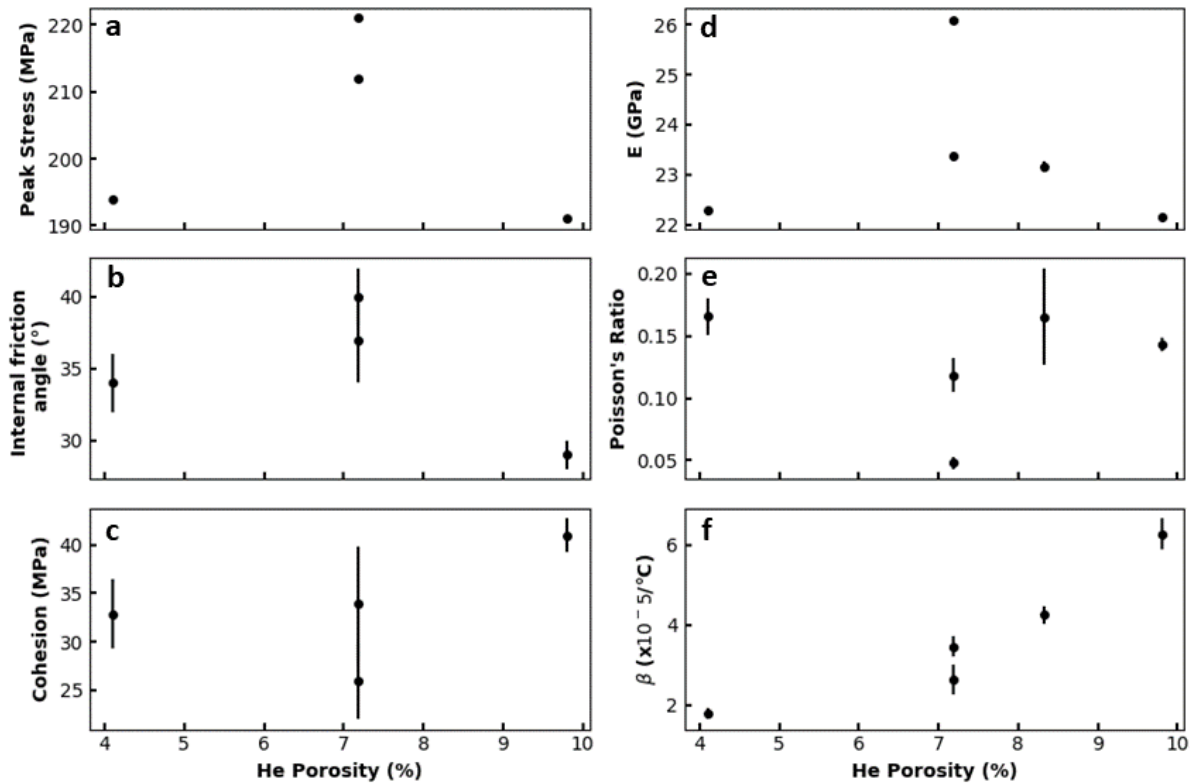


Figure 16: Peak differential stress (a), angle of internal friction (b), cohesion (c), Young's modulus (d), Poisson's ratio (e) and volumetric thermal expansion coefficient (f) as a function of initial He porosity.

As illustrated in Figure 16, the mechanical parameters do not show a clear correlation with porosity. The Young's modulus (22-26 GPa) and Poisson's ratio (0.14-16, 0.05 being an outlier resulting from the technical problem on the LVDTs during the test) are consistent with other sandstones of similar porosities and depths (Heap et al. 2019; Pijnenburg et al. 2019; Soustelle et al. In prep). The peak differential stresses (190-220) are significantly higher than those obtained from the common uniaxial compressive strength test (UCS) as the compressive strength of sandstones increases linearly with confining pressure (e.g., Lu et al. 2019). Unfortunately, there is no data on Mohr-Coulomb criterion parameters for intact Buntsandstein sandstones that we can directly compare. However, our data remain consistent with sandstones of similar porosity (cf., (Hackston & Rutter 2016), and references therein) despite the lack of accuracy of our direct method: the direct measurement of the failure angle.

Unlike the mechanical parameters, the coefficient of volumetric thermal expansion is consistent with the expected for sandstones (Somerton 1992; Soustelle et al. In prep) and seems to show a positive correlation with porosity. It should be noted that the highest value at the highest porosity corresponds to ELFO\_4a which has been tested at low  $P_e$ .

Figure 16 shows that the mechanical parameters depend on the sample depth. Indeed, we see that the Young's modulus, peak differential stress and angle of internal frictions increase while the cohesion decreases with depth. Unexpectedly, these trends suggest that the variations in depth are related to burial history rather than lithology.

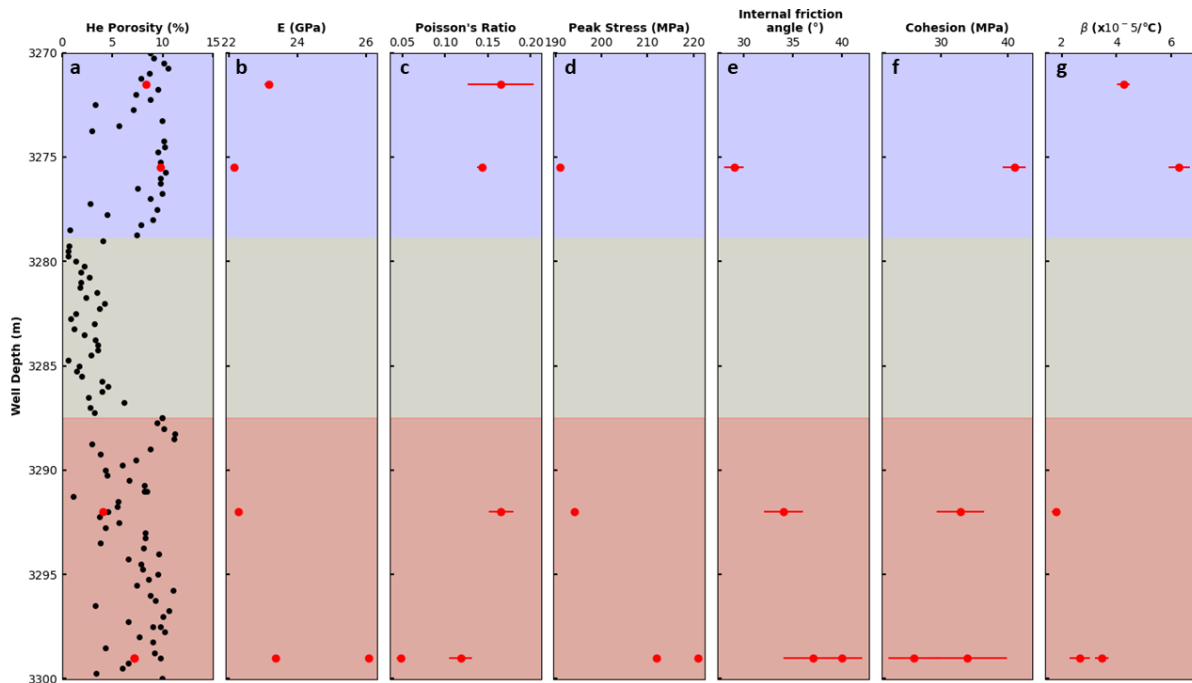


Figure 17: He porosity (a), Young's Modulus (b), Poisson's ratio (c), Peak differential stress (d), angle of internal friction (e), cohesion (f) and volumetric thermal expansion coefficient (g) as a function well depth. Red dots: studied samples, black dots: previous analyzes. Blue area: RBMVU, green area: RBMVC, red area: RBMVL.

While  $E$  decreases with depth,  $\nu$  and  $\beta$  increase it is therefore difficult here to predict the stress variation behavior due to thermoelastic stressing with depth. Similarly, the cohesion and angle of internal friction display an opposite behavior so prediction on SCU cannot be directly extracted from the experimental results. A thorough analysis of the stress conditions along the borehole depending on depth, temperature variations and boreholes orientations is required. The borehole stability will be investigated in WP3 through a numerical modelling approach partially based on the thermomechanical parameters measured and presented in this chapter.

## 2.4. Thermal Conductivity

Thermal conductivity has been measured in lab conditions for many of the prominent formations of interest to Netherlands subsurface exploration. Dalby et al 2018 measured rock properties from core samples throughout the Netherlands and summarized the results of Tertiary, Cretaceous, Jurassic, Triassic, Permian, Carboniferous and Devonian aged rocks. Eavor-Loops at Tilburg will target the Lower German Triassic, and samples from the Detfurth and Volpriehausen will be the focus of this report.

The Hardeggen Formation, Detfurth Member, and Volpriehausen members form a high net to gross sandstone package between 160m to 180m in the AOI. Primary horizontal development at Tilburg is twofold, as two sets of laterals are required and spaced at 75m. The Lower Detfurth sandstone member is the target of the uppermost set of laterals, and the Lower Volpriehausen Sandstone Member is the target of the lowermost set of laterals. To form the connection of laterals, the lowermost legs are angled up to intersect the uppermost legs at the toe of each horizontal leg.

Dalby 2018 collected analogous samples from the Lower Detfurth via cores obtained from WED-03 and WWN-03. In total, 8 samples were collected from the Detfurth and thermal conductivity was measured at ambient conditions. The resultant geometric horizontal saturated thermal conductivity ranges from 4.145 W/m·K to 5.385 W/m·K, which yields a geometric mean of 4.681 W/m·K.

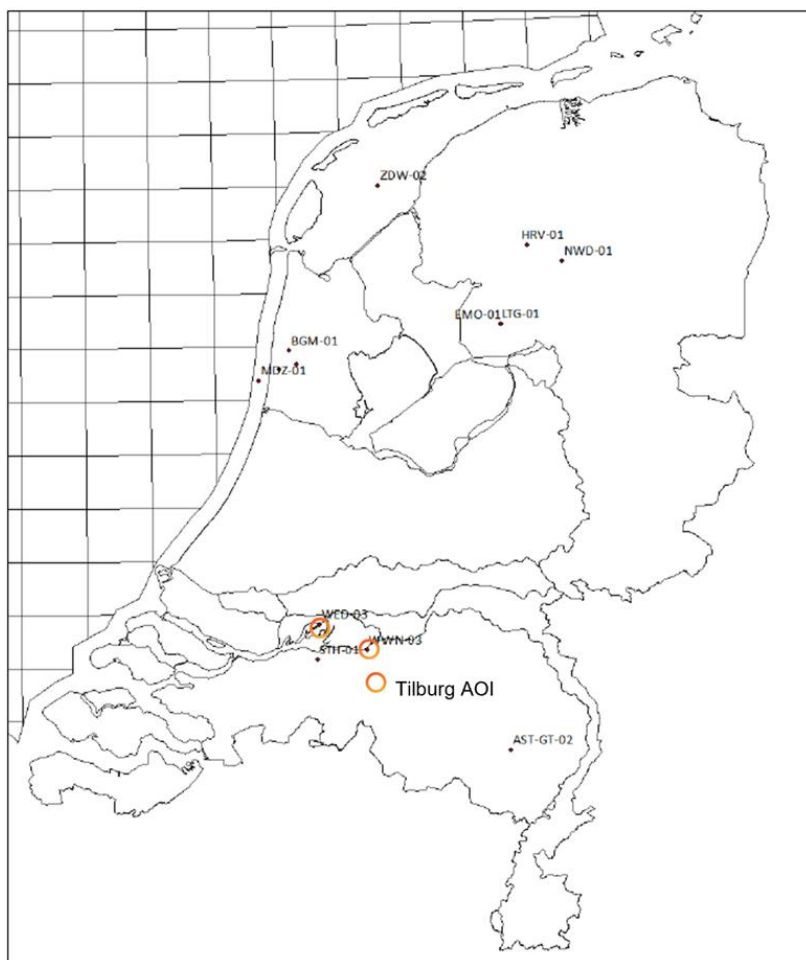


Figure 18: Map of reference wells WED-03 and WVN-03 relative to Tilburg AOI (modified from Dalby 1998)

Dalby 2018 also collected one analogous sample for the Lower Volprieausen sandstone via core obtained from STH-01. Although the sample size is limited, the thermal conductivity measured from STH-01 produces a horizontal saturated geometric mean thermal conductivity of 4.86 W/m·K. Dalby 2018 also measured samples from the Lower Volprieausen in Northern Netherlands from BGM-01. However, these samples have a higher feldspar content and are not representative of the Lower Volprieausen (Dalby 2018) at Tilburg. In wells HBV-01 and WWS-02, the Volprieausen was described as quartz rich with clay & iron constituents, filled with carbonate & dolomitic cement. It is difficult to assume that the single Volprieausen sample from STH-01 is representative as the data set is not robust. If all German Triassic samples are considered from Dalby 2018, the average thermal conductivity is 3.88 W/m·K (geometric) and 4.11 W/m·K (arithmetic) with a range between 2.974 to 5.39 W/m·K. From the data referenced above, an average thermal conductivity of 4.0 W/m·K is assumed for the Volprieausen Member.

The sandstone rich Hardeggen, Detfurth and Volprieausen packages are 160m thick at HBV-01 and 180m thick at WWS-02. A thin 2-3m Volprieausen claystone member exists at both HBV-01 and WWS-02 although at varying stratigraphic depths. It is possible that this clay rich member is not correlatable between the two main offsets at Tilburg. Still, the upper German Triassic sandstone package is approximately 60% of the overall package, and the lower German Triassic sandstone is 40% of the package. Assigning these ratios, the overall thermal conductivity of the Lower German Triassic is 4.40 W/m·K at ambient conditions

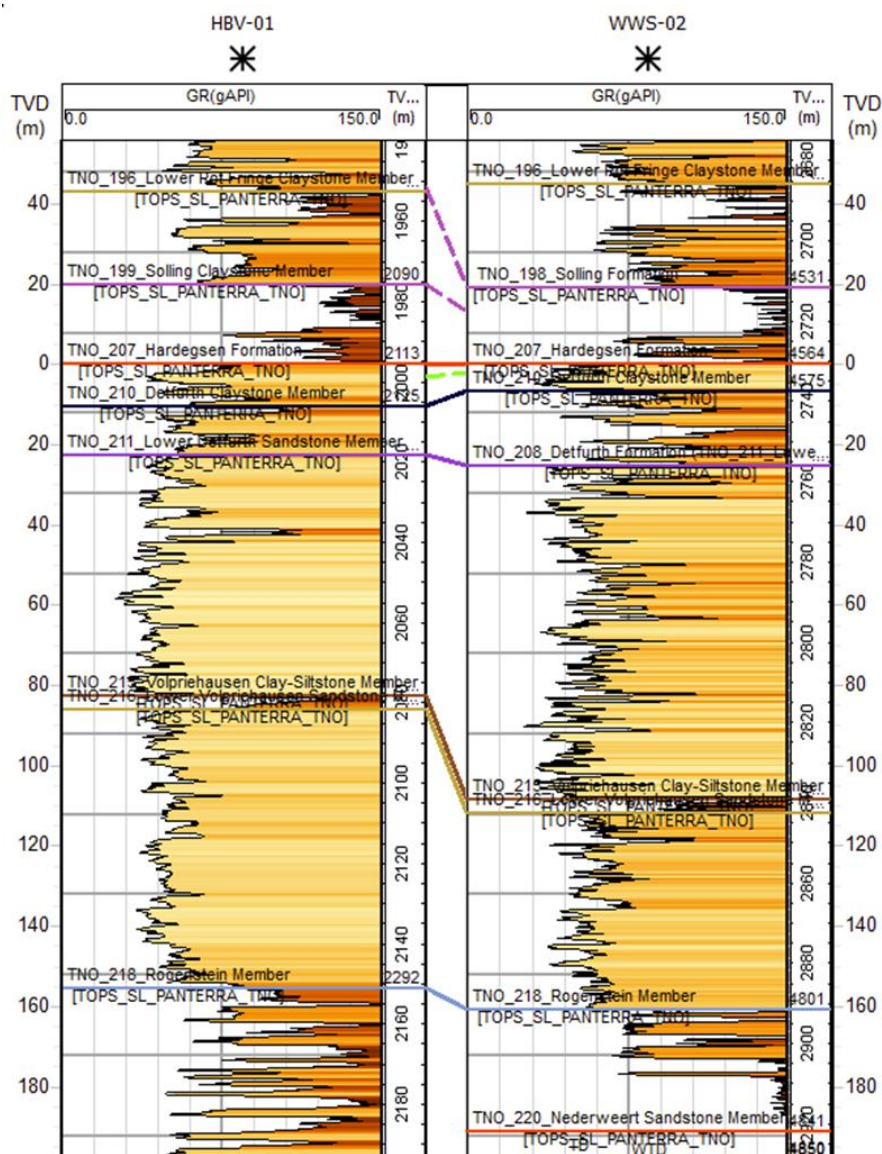


Figure 19: Gamma ray logs for the selected wells in the sandstone rich zones, showing different zonations

Using the mineralogical composition indicated in Table 6 an estimate can be made of the thermal conductivity of the target aquifers using average thermal conductivity values for the minerals. <sup>[1]</sup> For the Hardegsen Formation this would be around 4.30 W/m·K, for the Detfurth formation around 4.70 W/m·K and for the Volpriehausen Formation 4.68 W/m·K. As the (Upper) Detfurth and Hardegsen Formation are very heterogenous throughout the area (more alternations with silts, clay and mudstones) these values are of course variable as well (see also Table 7)

Table 7: Thermal conductivity estimates for the Main Buntsandstein

	Quartz	Feldspar	Plagioclase	Anhydrite	Dolomite	Siderite	Pyrite	Illite	Chlorite	Kaolinite	(W/m/K)
Hardegsen	47.3%	3.3%	2.4%	13.3%	14.3%	1.1%	0.8%	13.3%	0.2%	4.0%	4.30
Detfurth	73.4%	3.4%	1.6%	1.0%	10.3%	0.2%	0.5%	6.2%	0.6%	2.9%	4.70
Volpriehausen	73.1%	3.6%	0.7%	1.7%	11.1%	0.3%	0.0%	6.6%	0.9%	1.9%	4.68
Thermal Conductivity (W/m/K)	4.99	6.77	2.31	4.76	3	19.2	0.05	5.14	1	5.5	

## 2.5. Geothermal Gradient and Heat in Place

The predicted temperature of the German Triassic has been determined using NLOG ThermoGIS and measurements from offset well data. The NLOG ThermoGIS is a valuable tool for predicting a wide range of reservoir properties at a given location. The ThermoGIS mapping tool can be used to visualize the overview of Heat in Place ( $\text{GJ}/\text{m}^2$ ) on a country wide scale (Figure 20). The overall predicted heat in place for Southern Netherlands is quite high compared to the Northern regions. The Tilburg area is predicted to range between 80 and 120  $\text{GJ}/\text{m}^2$  as remnant heat near the Eindhoven area trends NW-SE towards Tilburg.

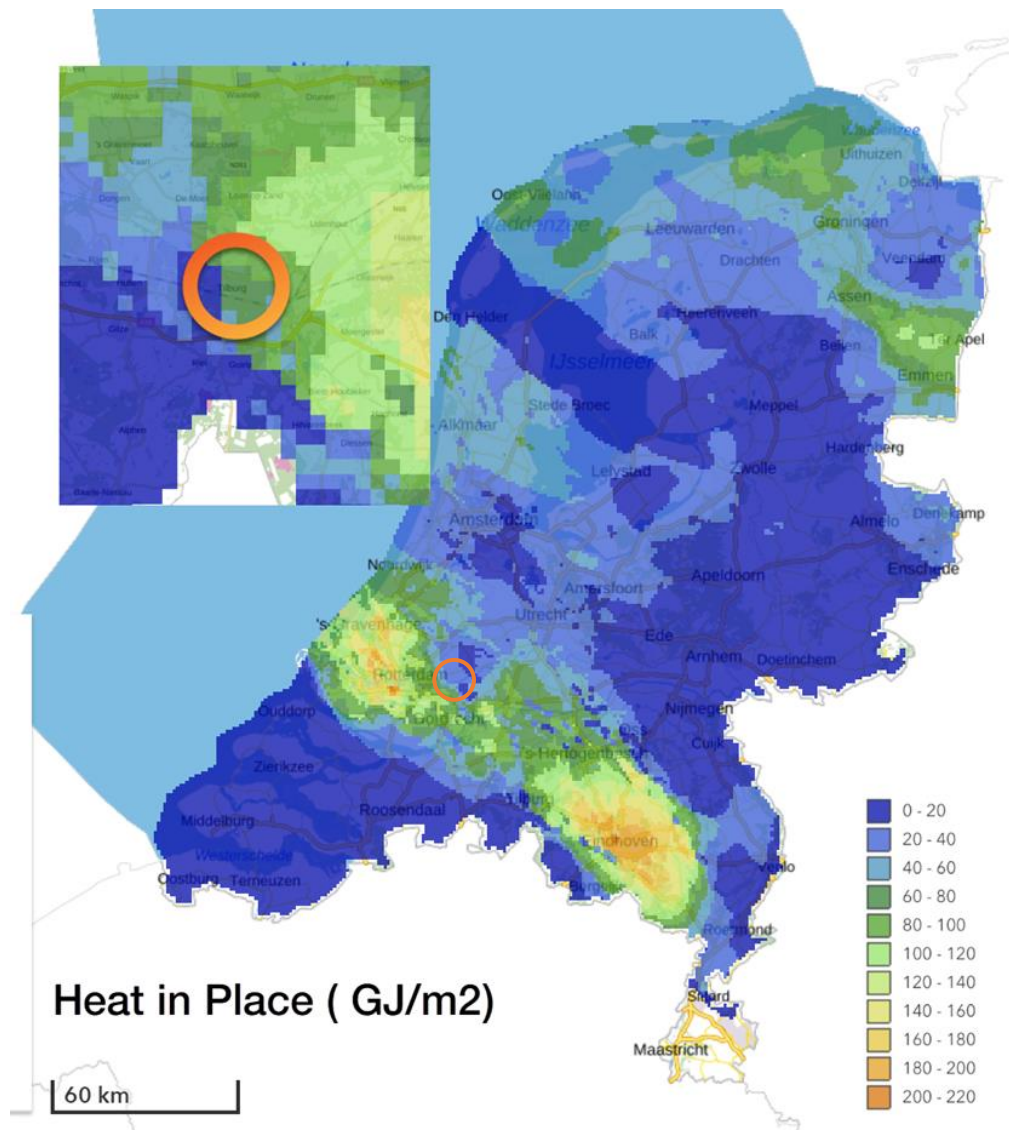


Figure 20: NLOG ThermoGIS overview map of heat in place for the Netherlands (ThermoGIS 2022)

The predicted temperature of the German Triassic has been determined using NLOG ThermoGIS and measurements from offset well data.

The ThermoGIS mapping tool can also be used to predict reservoir temperatures for any given formation in the Netherlands subsurface. For the AOI of Tilburg, the top of the Upper Volpriehausen

sandstone member has been mapped at 120°C at a depth of 3,398m TVD. Given an 8°C ambient surface temperature, the geothermal gradient is predicted to be 32.4°C/km (Figure 21).

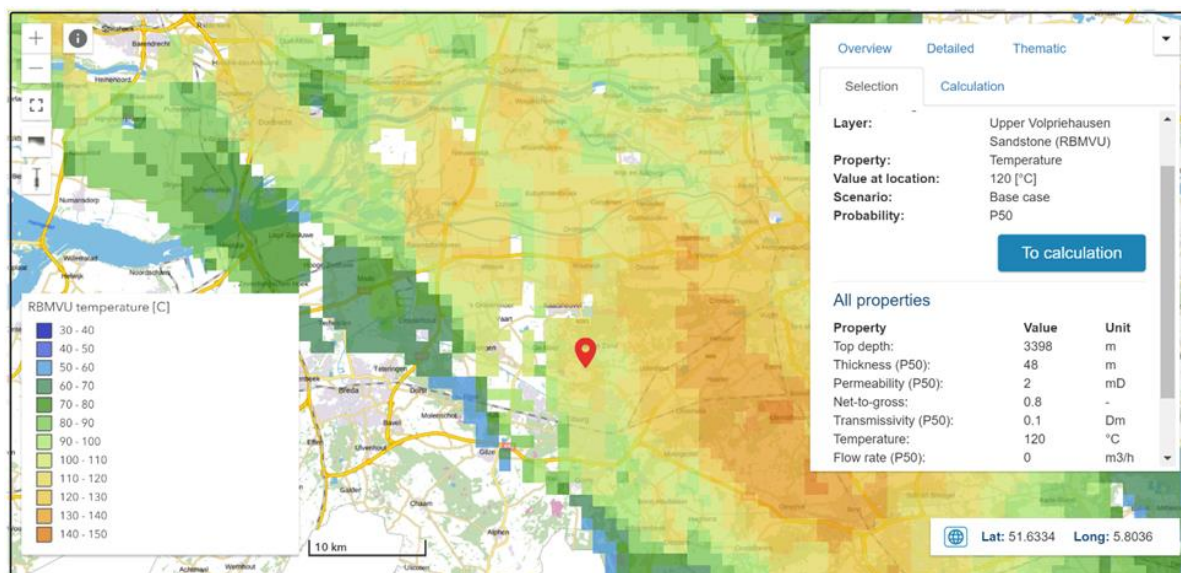


Figure 21: Reservoir temperature map (base case) of the Upper Volpriehausen Sandstone (RBMVU) in Southern Netherlands, placemark on map indicates Tilburg project location

Finally, the bottom hole temperatures for five nearby offset wells were analyzed for local geothermal gradient (Table 8). The geothermal gradient for all offsetting wells ranges from 32.8 to 35.5°C/km. The nearest offset, WWS-02, exhibits a 35.5°C/km gradient after 1500 hours of shut-in time, indicating the geothermal gradient could be higher than the ThermoGIS mapping tool suggests.

To summarize, a 32.4°C/km gradient is assumed to be the lowest expected gradient and 35.5°C/km is expected to be the high case.

Table 8: Temperature and Depth measurements of Tilburg offset wells indicating range of geothermal gradient values

Well name	Measured depth (m)	TVDss (m)	Temp. (°C)	Shut in time (hours)	Stratigraphy (formation)	Stratigraphy (group)	Geothermal Gradient (°C/km)
BKZ-01	2702	2672.4	98	1985	RBSHR	RB	32.9
WWK-01	3802	3079.3	113	1395	RBSHR	RB	33.5
WWN-02-S3	3968	3054.5	115	600	RBSH	RB	34.4
WWS-01-S1	3485	3031.7	108	1274	RBSHR	RB	32.3
WWS-02	4850	2929.0	114	1500	RBSHN	RB	35.5

## 2.6. Subsurface 3D Geological Model

A subsurface 3D geological model was built using the AspenTech SKUA-GOCAD software and used as input to the MACRIS modelling methodology using Schlumberger Petrel software. The AOI of the 3D geomodel covers a 70.4 km<sup>2</sup> area of the main structural components within the Tilburg area. In total, 76 faults were interpreted from the seismic AOI and imported both as fault sticks and surfaces into SKUA-GOCAD. At this stage, a total of nine reference seismic depth horizon grids were also imported into the geomodel. All seismic data products were imported in the depth domain, as time-depth relationships are predefined as documented in section 2.1.5.

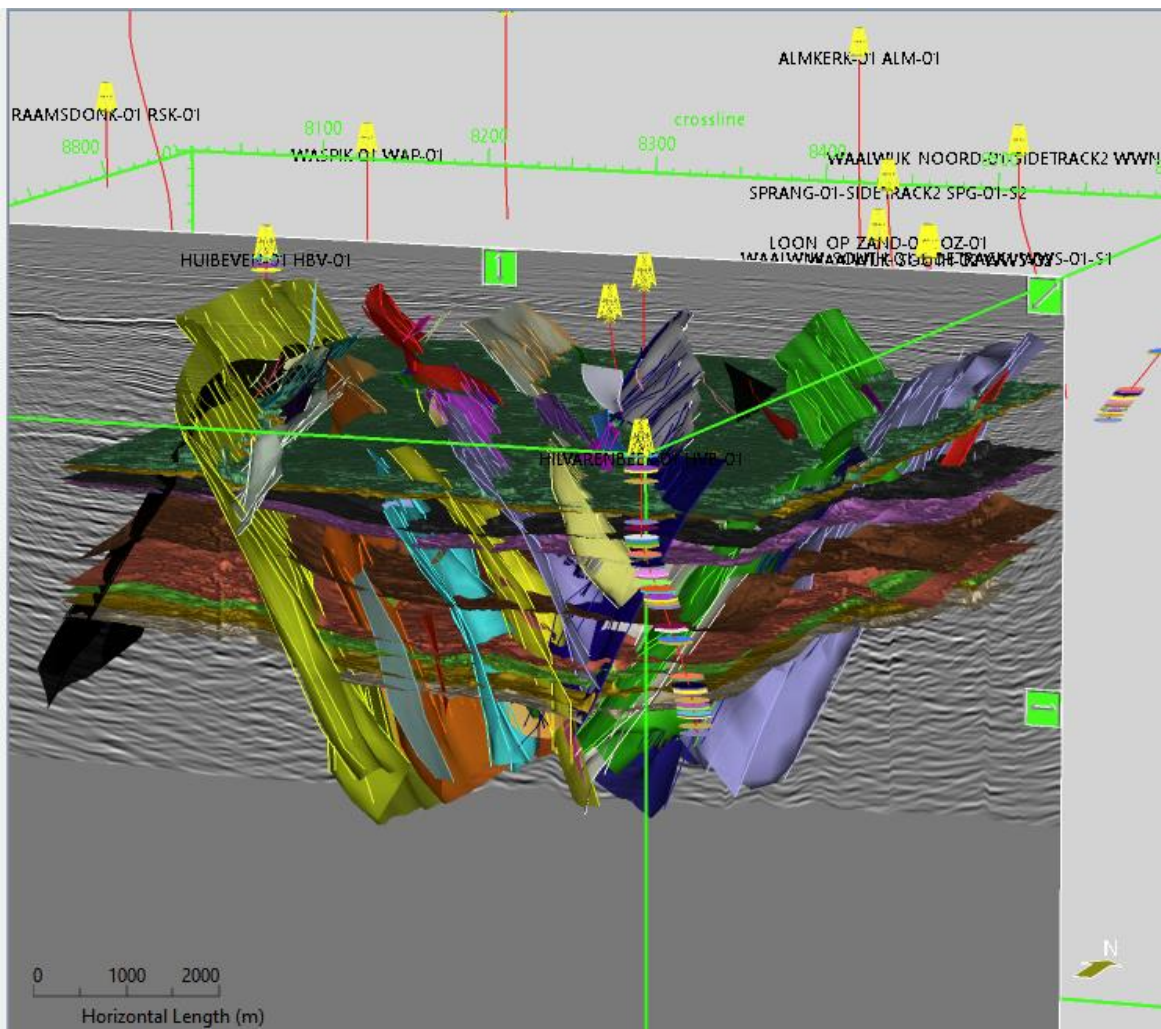


Figure 22: Raw geoscience data prior to completing 3D geological modelling workflow

The fault relationships must be correctly represented in the geomodel to honor the structural setting of the Tilburg area. The area is predominately characterized by N-S striking normal faults expressed in master graben faults, branching antithetic normal faults, and crossing normal faults. In general, the major faults exhibit large offsets typically ranging between tens to hundreds of meters of displacement. The minor antithetic and smaller normal faults typically show minor offsets less than tens of meters, or minor lineations characterized by no observable offset.

Horizons within the 3D geological model use input data both from the seismic interpretation and well formation top markers of HBV-01 and WWS-02.

Faulting observed at the Triassic Bunter sandstone stratigraphic level is dominated by normal faults striking N-NW to S-SE with large offsets to the West and East of the main Tilburg graben. Intra-graben faulting is dominated by normal faults with little to no visible offset. The small intra-graben faults typically strike N-NW to S-SE and occasionally W-NW to E-SE.

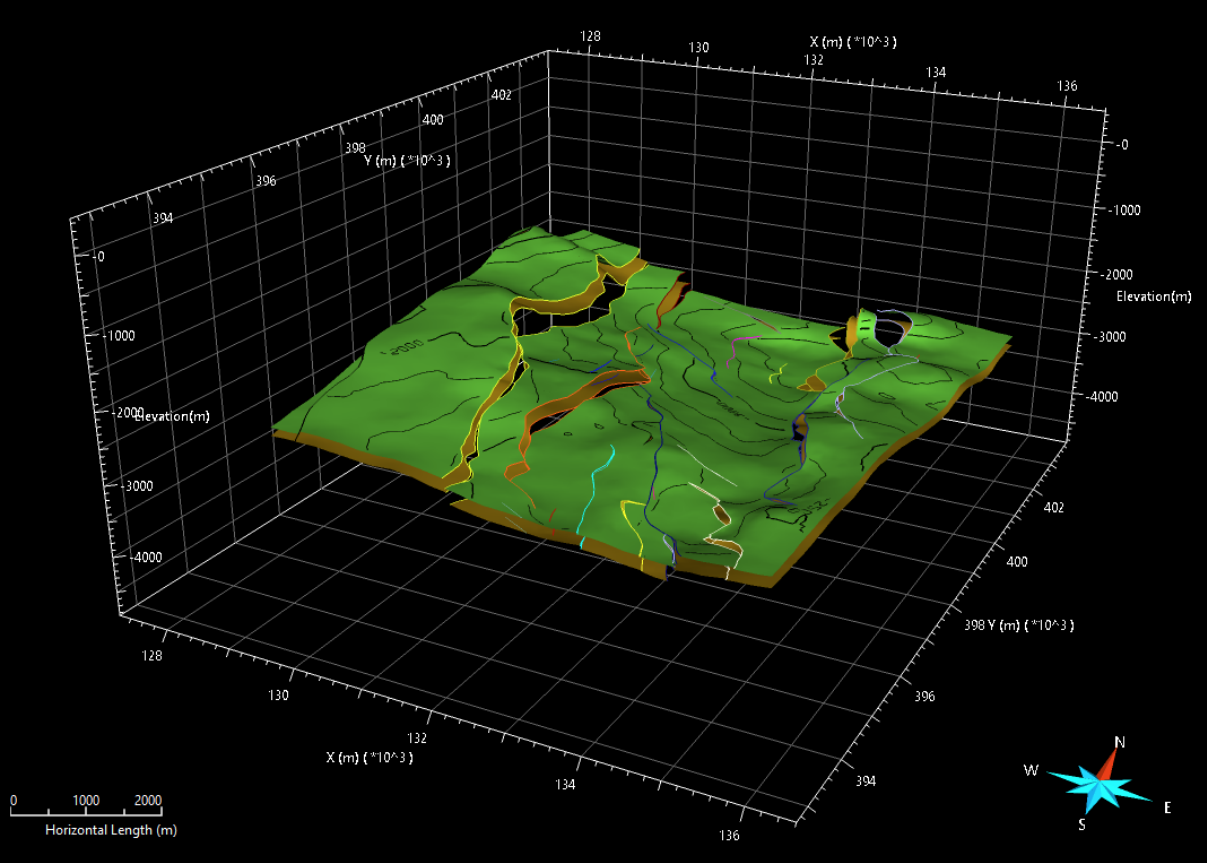


Figure 23: Structure of the Top Lower German Triassic sandstone unit (green contoured) showing variable offsets of intersecting faults (colored polylines on structure) 1x VE.

Upon completion of the full structural model, a simulation grid must be prepared for dynamic modelling of thermal changes and stress perturbations due to Eavor-Loop operations. These conditions will be assessed in WP3 - Thermal changes and borehole stresses due to EL exploitation. Generating a simulation grid in SKUA-GOCAD converts the complex unstructured mesh of the 3D geological model into a traditional “sugar-cube” style fixed dimension grid. The output simulation grid exhibits the following geometry

Geometry	100m x 100m x 25m
Total cells / Active cells	2,448,888 / 507,496
Fault model	Stair Step

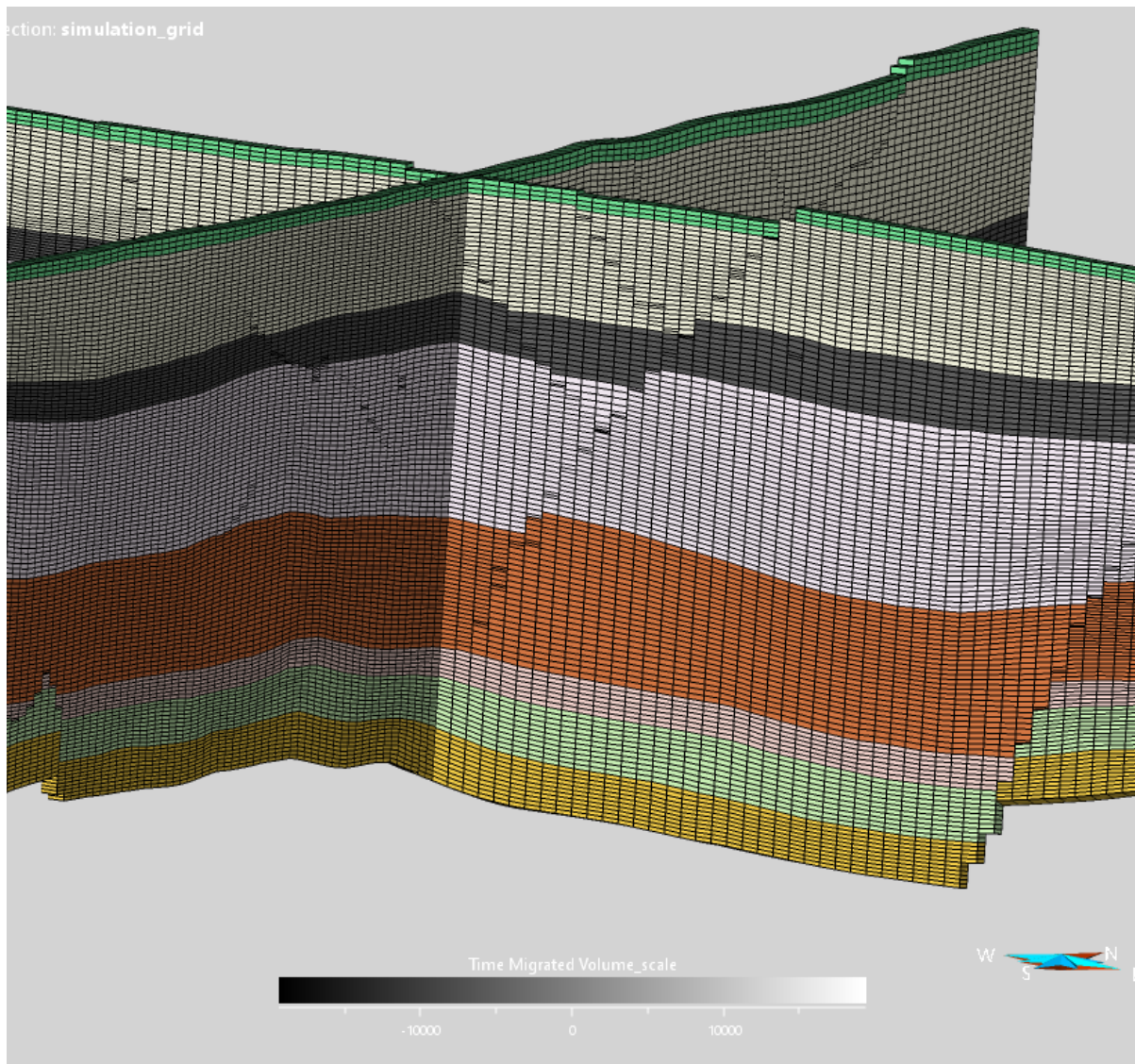


Figure 24: Defined 100x100x25m grid cell size of the simulation grid depicting stair step fault geometry and true geological structure.

## 2.7. Eavor-Loop location & design

### 2.7.1. Project Location

For Eavor-Loop district heat projects, the selection of a surface location for drilling and production operations is critical as it must consider several factors:

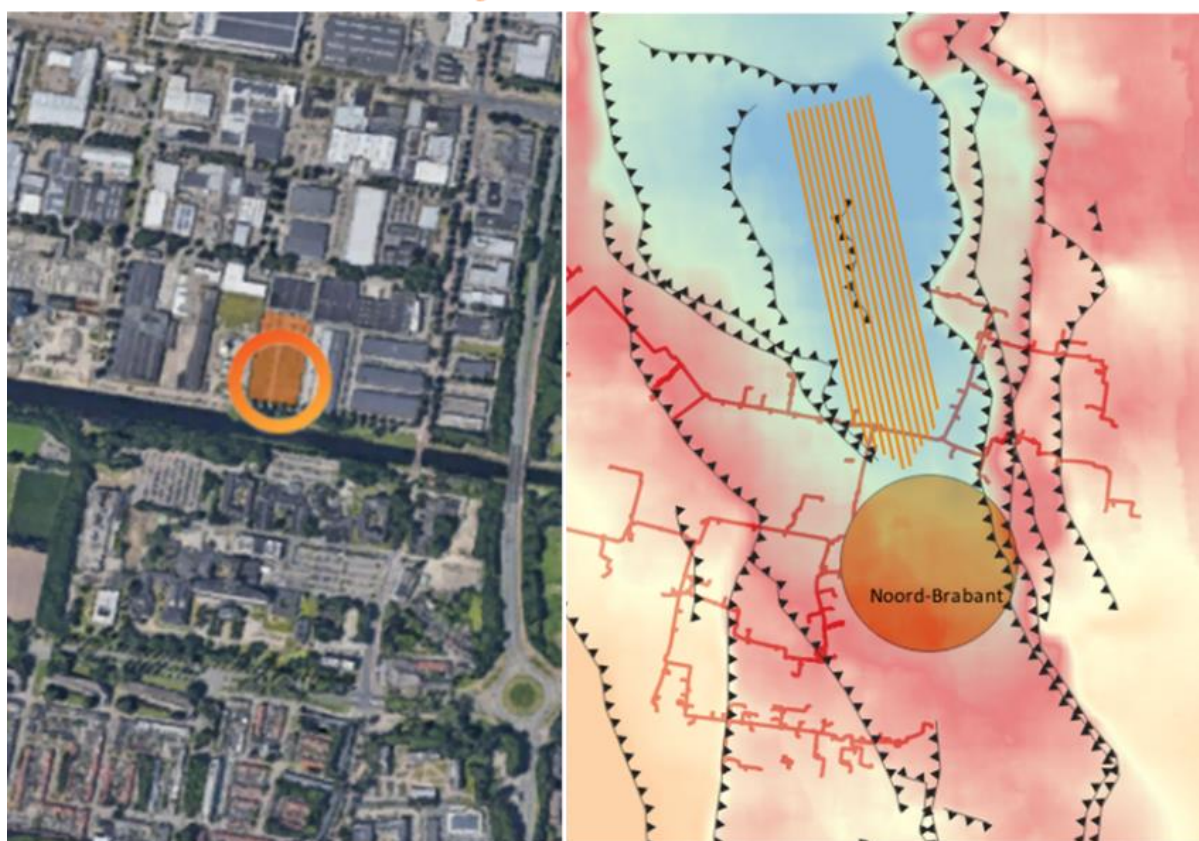
- Suitable subsurface conditions
- Availability and current use of land (industrial, residential, etc.)
- Proximity to Amer heat network piping

Subsurface selection criteria include target formation depth, temperature, formation rock type and mineralogy, and faulting, among others. Unfortunately, the top areas for Eavor-Loop subsurface placement result in an unsuitable surface location. Proximity to a suitable tie-in heat network tie-in point and the current use/availability of land is often a trade-off as suitable drilling locations within the built environment can be challenging to find. However, moving away from the built environment

and the heat offtake customers will result in larger capital costs to build new connections to the heat network.

An Eavor-Loop drilled from South to North would follow a downdip Bunter Sandstone target formation. The resultant horizontal radiator section would require an 85° drilled inclination to follow the downdip structure. Drilling horizontally with a slight downdip trend would aid in torque and drag during drilling and result in a predicted horizontal length of 3,000m. Unfortunately, this placement results in a surface location directly in Tilburg city where land availability is very scarce and directly adjacent to the population which raises noise concerns while drilling. The approvability of acquiring land in this area is very low.

## City Location

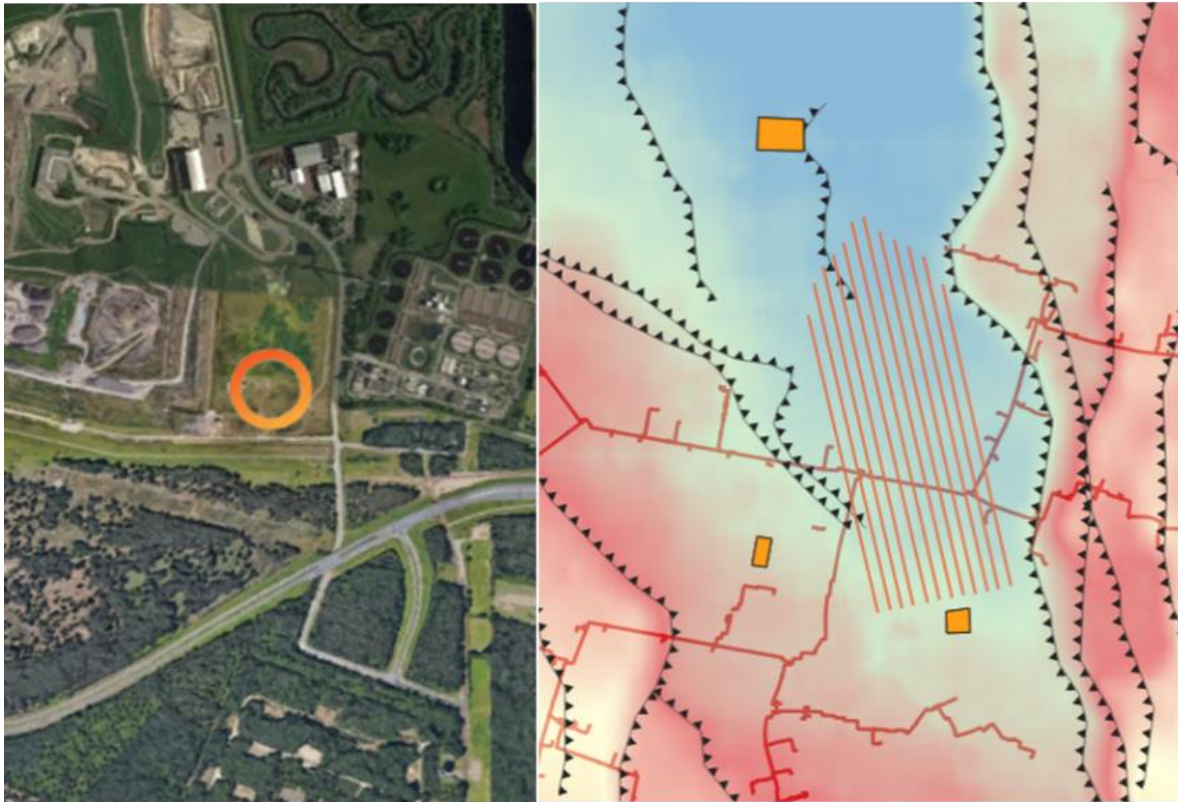


12 x 3,000 m laterals

Figure 25: Scenario of Eavor-Loop placement following downdip structural plunge yields horizontal lateral lengths of 3,000m. This scenario requires land acquisition in a densely populated area and as a result is an unrealistic scenario.

A second configuration was considered and eventually selected for an Eavor-Loop in Tilburg. An Eavor-Loop drilled from North to South was then considered to access land outside of Tilburg city limits. As the Tilburg Graben is dipping from South to North, an Eavor-Loop drilled from the North industrial area would require drilling the resultant horizontal radiator section updip at approximately 95°. As expected, drilling horizontal with a slight updip trend has the opposite effect of drilling downdip. Lateral lengths are reduced due to the higher modelled torque and drag resulting in a predicted horizontal length of 2,100m. This second scenario was selected as documented in this section.

## Industrial Park



12 x 2,000 m laterals

Figure 26: Scenario of Eavor-Loop placement following updip structural climb yields horizontal lateral lengths of 2,100m. This scenario is preferred from a land acquisition standpoint as land is more readily available than in the city scenario. However, drilling updip horizontally is more challenging and results in shorter lateral lengths than the downdip scenario due to higher modelled torque and drag.

A drilling and production site, located in an industrial area on the north side of Tilburg (depicted by the orange loop in Figure 26), was chosen based on: acceptable subsurface considerations, a tie-in distance of approximately 1.5 km to the Amer heat network, and minimal disturbance to residents or businesses during construction and operation. The parcel of land selected for the Project is owned by Attero, a waste management company with several sites located across the Netherlands and is not currently in use. A bioenergy facility is currently under construction immediately to the North of the selected land, and the whole area has been designated as a renewable energy zone.

The following figures show the project location in relation to the built environment, the heat network, and the geothermal license area. Figure 29 projects the lateral wellbores of the Eavor-Loop from the subsurface and overlays them on top of the build environment.

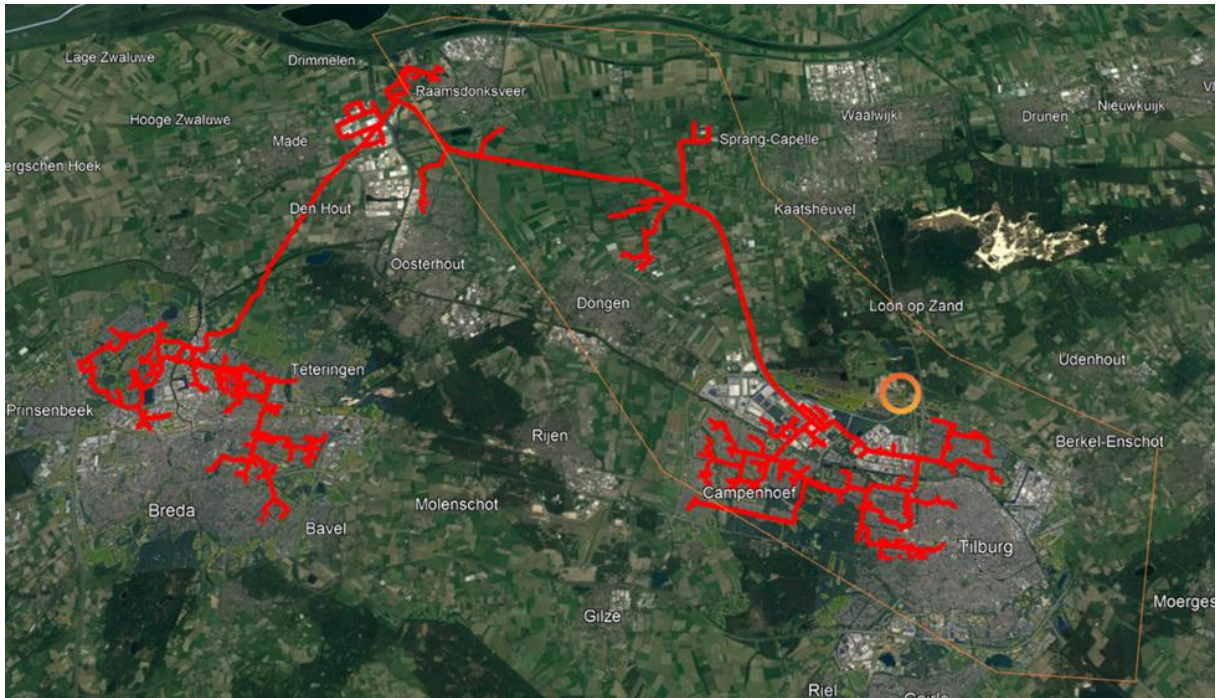


Figure 27: Amer heat network with the Tilburg Eavor-Loop location shown in orange circle



Figure 28: Project location and Amer heat network.

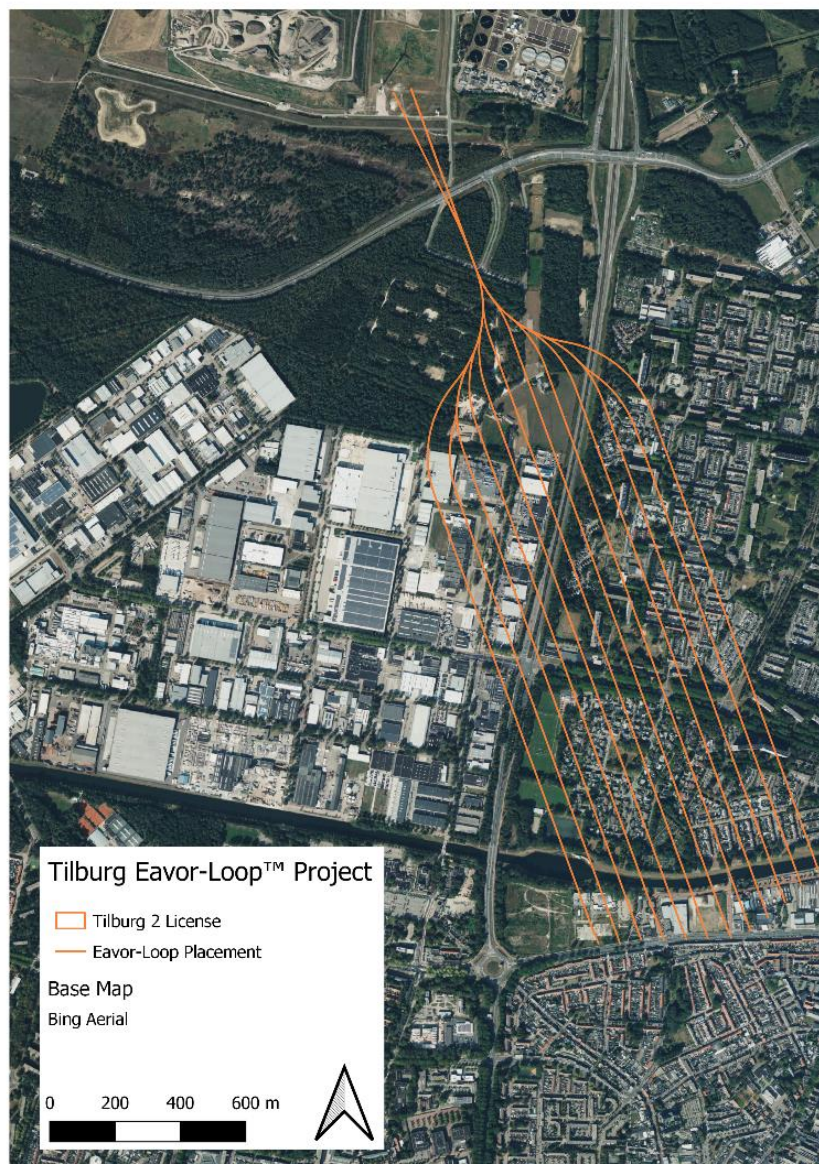


Figure 29: Subsurface laterals projected onto the surface.

### 2.7.2. Eavor-Loop Design

The Eavor-Loop is constructed using two drilling rigs which each complete one vertical well and 12 lateral legs. During drilling operations, which are expected to take six to seven months, a surface footprint of approximately 120 m x 110 m is required to accommodate both rigs and associated drilling services. The planned rig orientation and equipment layout is shown in Figure 29.

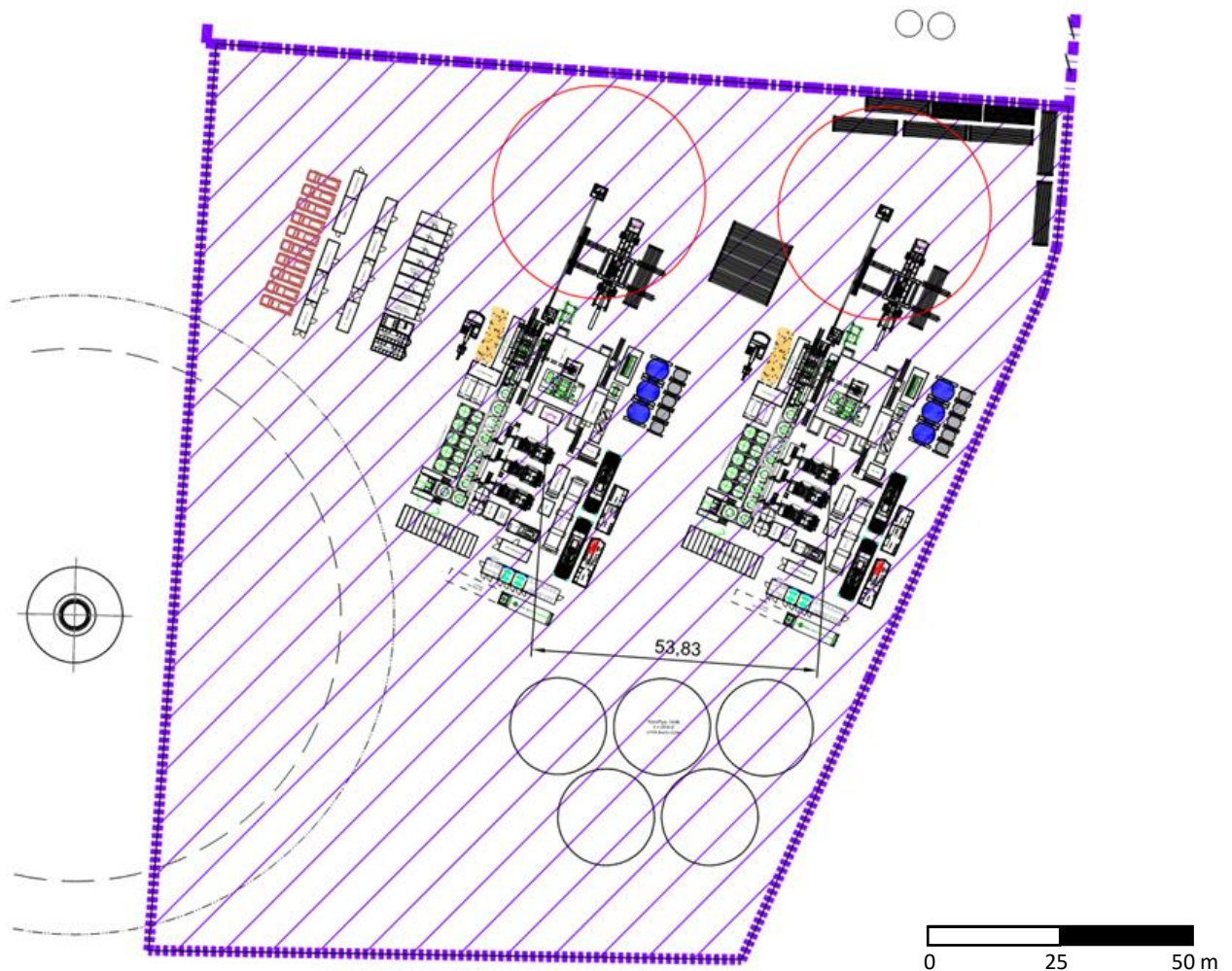


Figure 30: Generic site layout during drilling operations with two drilling rigs

In this orientation, the inlet and outlet wells are located approximately 54 meters apart. It is important to note that the layout of the drilling rigs and equipment can be shifted depending on site specific requirements.

Upon the completion of drilling operations, the rigs will be moved off of from the location and production facilities will be constructed. The facilities will consist of the following:

- Evaporator-Loop working fluid circulation pump
- Pressure vessel
- Working fluid Hold-Up tanks
- Plate and frame heat exchanger
- Heat pump

The total surface area required for the 30-year producing life of the Project is approximately 54 m x 43 m. A preliminary facilities layout is shown in Figure 30. As with the drilling rig orientation, the layout of the production facilities can be shifted to accommodate site-specific needs.

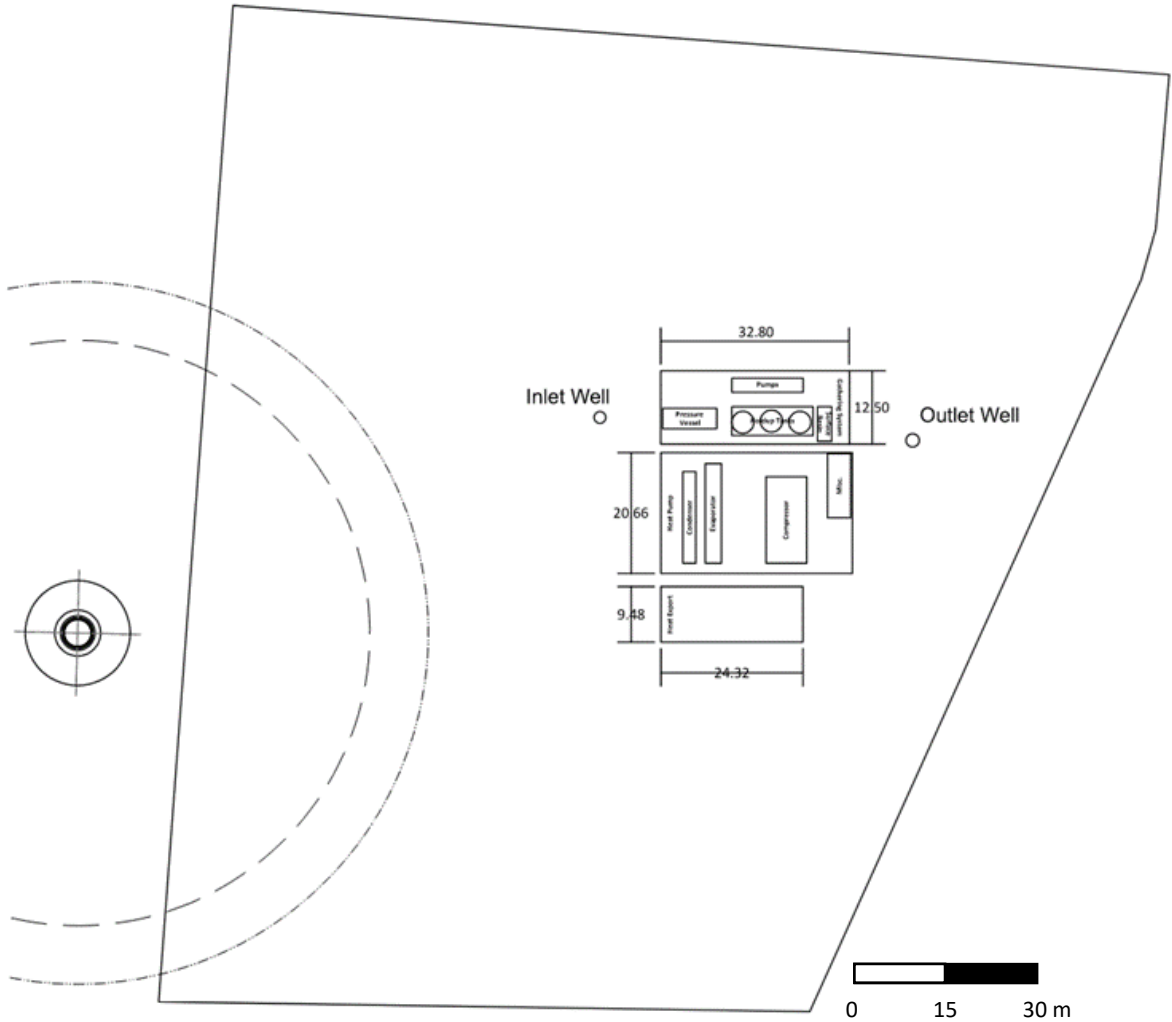


Figure 31: Layout of Eavor-Loop production facilities

The commercial Eavor-Loop 1.0 design is constructed with two drilling rigs operating simultaneously from one surface location. First, the vertical well section is drilled, and the intermediate casing is cemented in place at both sites according to standard industry regulatory practice. Then, two deviated wellbores are drilled out of each standard vertical cased well and intersect at the “toes”, at the end of the approximately 2,100 m lateral length. The intersection is completed with magnetic ranging technology to sense the target wellbore with sufficient accuracy to intersect directly. This process is repeated until all multilateral wellbores are intersected, and the system is then completed using the Rock-Pipe chemical completion method and tested to ensure an appropriate seal.

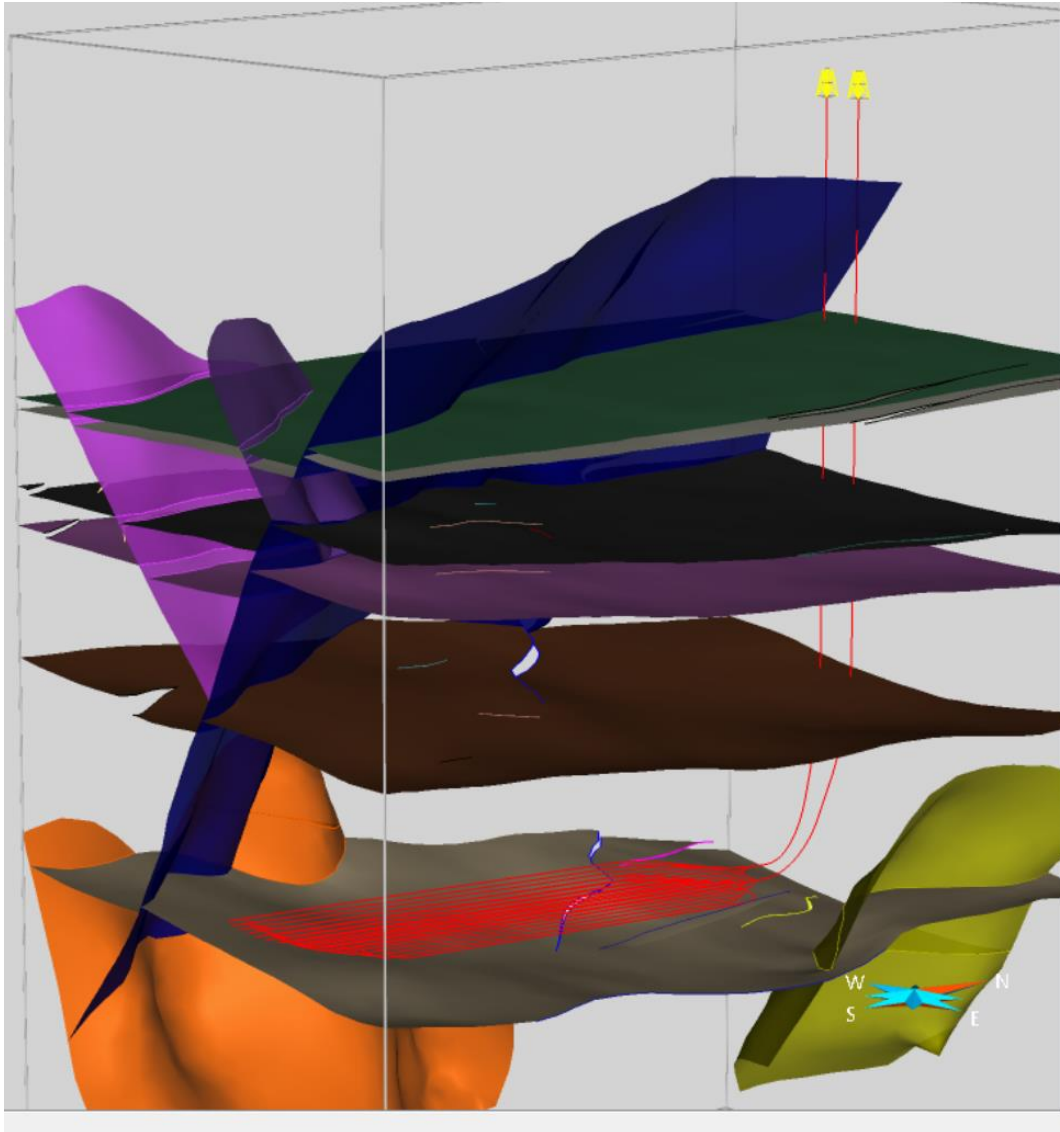


Figure 32: Vertical to the horizontal well profile of the Tilburg stratigraphy VE = 1x

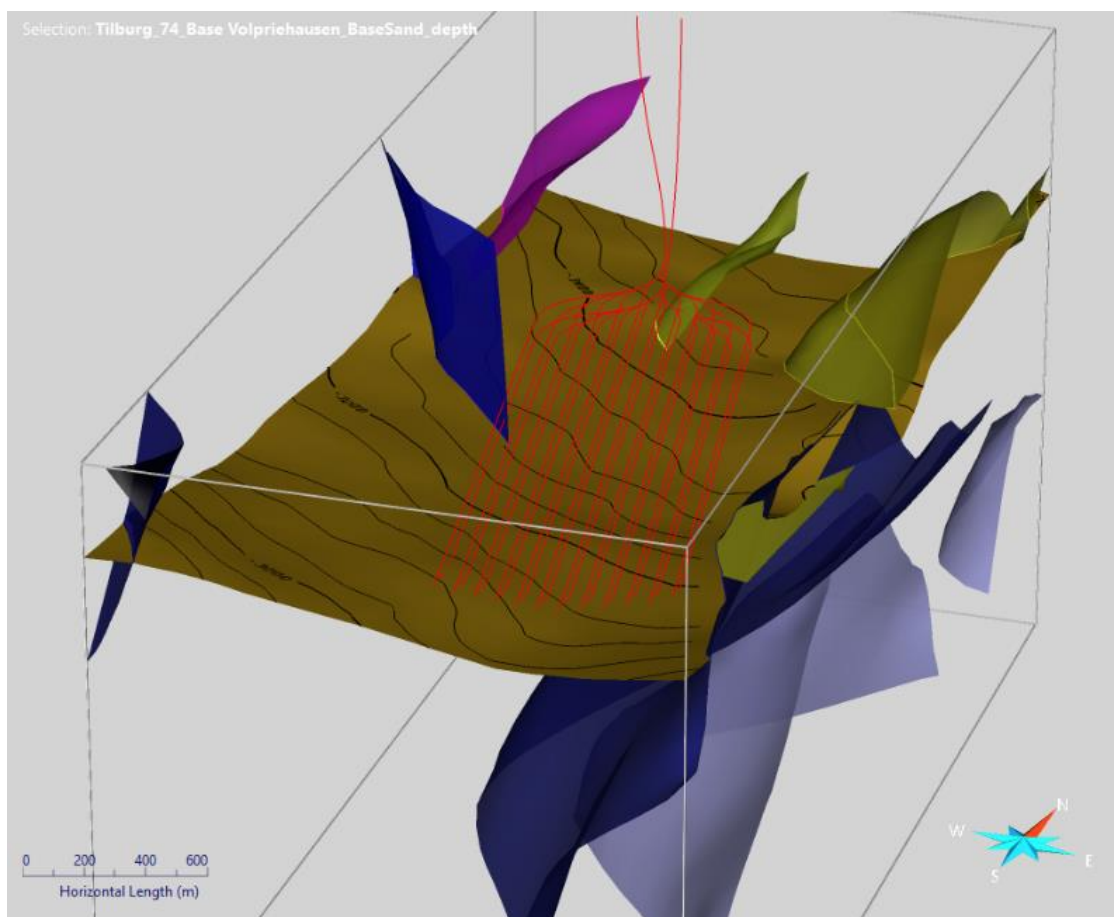


Figure 33: Lateral Eavor-Loop placement within the Lower German Triassic sandstone package. Structural maps depict the Base Volpriehausen sandstone structure. Colored surfaces indicate faults including two sub-seismic resolution lineations (yellow and blue) crossing the Eavor-Loop

After well construction, the drilling fluid is replaced with a working fluid designed for improved operational performance. Eavor-Loop™ is an “advanced geothermal system” but is unique from traditional geothermal and Enhanced Geothermal Systems (EGS) in several critical aspects, as outlined in Table 9 below.

Table 9: Comparison of Traditional Geothermal and Eavor-Loop Technology

Traditional Geothermal	Eavor-Loop™
Open system – water flows through the reservoir, and fluid exchange between the system and reservoir	Closed system – working fluid circulates in isolation of the reservoir, with no fluid exchange
Requires a permeable aquifer and hot convective zone	A permeable aquifer is not required, and exploration risk mitigated
Requires an electric pump to bring the brine to the surface, parasitic load	Driven by natural thermosiphon, no pumping required*

It can require fracking to increase flow, the potential for induced seismicity	No need for fracking, no induced seismicity
Can produce GHGs and CO <sub>2</sub> with produced brine	No GHGs or CO <sub>2</sub>
Continuous water use and on-going treatment and/or disposal required	Minimal continual water use, no production brine requiring treatment or disposal
OPEX can be greater than CAPEX over the life of the project	OPEX is ~80% less than traditional geothermal
Large uncertainty and risk in thermal output	Low uncertainty and risk in thermal output
Project cycle time is typically 5 to 10+ years	Project cycle time ~2 years
Baseload, not dispatchable	Baseload and dispatchable

*\*Note – While the system can operate within the thermosiphon window, a circulation pump may be added to optimize temperature and or heat output to meet offtake demand*

## 2.8. Thermal output

The thermodynamic modelling tools developed by Eavor (and validated through the operation of the Eavor-Lite as well as by independent third parties) are suitable for any Eavor-Loop configuration regardless of rock type. The thermodynamics of the system are calculated at discrete intervals along the wellbore, with the exact same physics and software being applied regardless of the well configuration or rock type, just using different inputs. The key inputs are the number of laterals, wellbore geometry (vertical and multilateral length, diameter), depth, formation temperature, and rock thermal conductivity. The values of these parameters for Tilburg are outlined in Table 10 below.

Table 10: thermodynamic parameter comparison for Eavor-Lite and Tilburg Loop systems

Parameter	Eavor-Lite	Tilburg
Number of Laterals	2	12
Depth, TVD [m]	2,400	3,275
Site-to-site distance [m]	2,500	Co-located, < 100 m (James Joyce)
Vertical casing size [in]	7	9-5/8
Multilateral wellbore size [in]	6-1/8	8-1/2
Rock Type	Quartz/Calcarenite Sandstone	Arkosic Sandstone
Formation Temperature [°C]	75	120

<b>Rock thermal conductivity [W/ m K]</b>	4.64	4.40
<b><math>\Delta T</math> Inlet to Outlet well [°C]</b>	30	30
<b>Multilateral completion</b>	Rock-Pipe	Rock-Pipe
<b>Multilateral Junctions</b>	Bent sub, time drill, no whipstock	Bent sub, time drill, no whipstock
<b>Intersection technology</b>	Magnetic ranging, blind approach	Magnetic ranging, visible approach
<b>Facility</b>	Storage tank, start-up circulation pump, aerial cooler, filters and throttle valve with control logic	Storage vessel, start-up circulation pump, filters and throttle valve with control logic, heat exchanger for district heating, ORC for power generation
<b>Porosity %</b>	9	4-6
<b>Matrix Permeability [mD]</b>	1-50	<0.1 – 25

The key input parameters to assess the heat transfer are the formation temperature and thermal conductivity, which have been investigated at depth for Tilburg as outlined in Sections 2.4 and 2.5. Another necessary input is the surface area across which the heat transfer can occur, which is accounted for by the number and length of the laterals and the overall geometry of the system. Lastly, the circulation rate of the fluid through the loop is defined. This is unique to a closed loop geothermal process as the circulation rate can be selected in advance, rather than dictated by the reservoir. The circulation rate is optimized for each well design to maximize the thermal output of the Eavor-Loop while also ensuring that the temperature and thermal capacity demands of the offtake customer are met.

Using this methodology, the thermal output of the Eavor-Lite project has been within 1% of the modelled values for the initial 2 years of operation (The same thermodynamic model that was successfully validated with the Eavor-Lite project was used to assess the thermal output of the Tilburg Project over a 30-year project life. While Eavor-Lite is indeed cooler and shallower than our planned commercial Eavor-Loops in Tilburg, the fundamental physics and thermodynamics governing the processes are the same. Eavor forecasts the Tilburg output using the same thermodynamic model that has been validated by over 3 years of Eavor-Lite data as well as numerous third parties, including van Wees (2021) of TNO, Netherlands, Beckers and Johnston (2022) of National Renewable Energy Laboratory (NREL) USA, Yuan et al. (2021) of Natural Resources Canada (NRCan), and Droessler et al (2020) of C-FER Technologies, Canada. These four organizations have audited Eavor’s internal thermodynamic model and concluded it is accurate in its estimation of Eavor-Lite and acceptable for extrapolation to other projects.

One of the key benefits of Eavor-Loop technology is that the thermal output of the systems can be calculated within a narrow range of certainty prior to construction and drilling operations. Unique from traditional geothermal developments where the key uncertainty is the production rate of the geothermal well, this circulation rate is designed for and controlled in Eavor-Loop systems.

### 2.8.1. Thermal Depletion / Degradation

An Eavor-Loop has remarkably consistent and predictable output over long timeframes. As heat is extracted from the earth the radius of the temperature affected area around the wellbore expands; beyond this radius the reservoir is still at virgin temperature. This radius is a logarithmic function of time, and the lateral wellbores have minimal interference with each other if spaced properly. Therefore, decline is addressed by calculating the effective radius and specifying lateral spacing requirements for the Project to ensure minimal wellbore interference. This spacing requirement is shown as  $\Delta x$  in Figure 34. This has been a consideration in determining the lateral spacing requirements, which have been specified as 65 m between horizontal laterals, and 75 m vertical spacing between the inlet and outlet set of lateral legs. The vertical spacing is dictated by the maximum placement to access higher rock temperatures while permitting ranging activities to take place and will typically be larger than the horizontal spacing as the horizontal spacing is governed by the thermal depletion consideration.

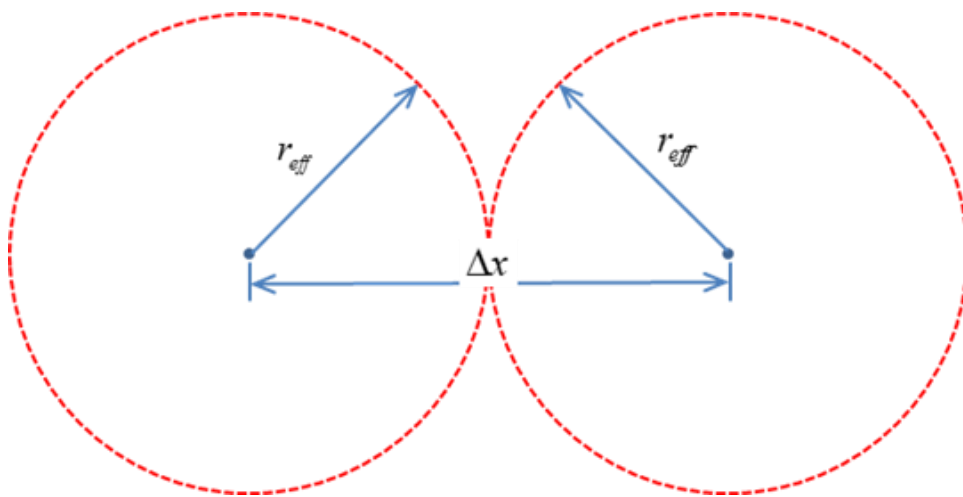


Figure 34: Schematic of effective thermal radius vs. spacing between two horizontal laterals to avoid heat transfer interaction.

WP3 will investigate the effective thermal radius specific to the subsurface conditions in Tilburg

### 2.8.2. P50 Energy Yield

For the purposes of the Eavor-Loop Tilburg Project this study, the Tilburg Eavor-Loop feasibility study, and the 2023 SDE++ application, Eavor's analytical model was used to predict the thermodynamic performance of the system. This methodology is in line with the conclusions from TNO's audit (van Wees 2021), which suggested that an analytical approach is favoured for SDE applications. For geothermal projects applying for SDE++ funding, a P50 estimate is required which is typically generated by the DoubletCalc program. As per TNO's recommendations van Wees (2021) in the Audit Report the analytical methodology used to calculate the conductive heat transfer across the length of the wellbore can be considered the P50 case.

Table 11 presents the P50 energy yield and process conditions expected for the Project.

Table 11: P50 Output Parameters

	Summer (Apr - Dec)	Winter (Jan - Mar)
Heat Grid Temperature (°C)	95	120
Eavor-Loop Outlet Temperature (°C)	89	102
Heat Exchanger Inlet Temperature (°C)	97	122
Heat Exchanger Outlet Temperature (°C)	66	66
Eavor-Loop Inlet Temperature (°C)	60	51
Working Fluid Flow Rate (kg/s)	70	30
<b>P50 Thermal Duty (MW)</b>	<b>9.1</b>	<b>7.1</b>

### 2.8.3. Surface Facilities and Process Flow Conditions

The purpose of the Project is to generate renewable heat for use by Ennatuurlijk in the Amer heat network. The design of the Eavor-Loop, both in terms of loop size and operating parameters, has been optimized to integrate with the existing heat network. As the heat network supply temperature has seasonal variation, the outlet temperature of the Eavor-Loop will be varied to ensure it is at least 2°C higher than the heat network temperature. This is accomplished by varying the working fluid flow rate of the system – as the flow rate is slowed down, there is more time for the working fluid to absorb heat from the surrounding rock in the radiator section of the loop, resulting in a higher temperature. Conversely, if the flow rate is increased, less heat transfer will occur resulting in a lower outlet temperature; however, as the energy produced is governed by Equation 1, the thermal duty will increase with increasing flow rate (and decrease with decreasing flow rate).

$$Q = m\dot{C}\Delta T$$

Equation 1: Thermal duty

Given the geological conditions of the license area, notably a 120°C bottom-hole temperature, a heat pump will be integrated with the Eavor-Loop system to ensure that the demand from the heat network can be met year-round. Including a heat pump with the Eavor-Loop is common for older heat networks that operate at higher temperatures, especially in areas with lower geothermal gradients. There are two main benefits of incorporating a heat pump:

1. The heat pump will boost the Eavor-Loop working fluid temperature to meet the temperature requirements of the heat network
2. The heat pump will increase the temperature difference between the inlet and outlet wells, which will result in a larger thermal duty

The main technical specifications of the heat pump are described in Table 12.

Table 12: Heat Pump Design Specifications

Variable	Value
Heat Pump Size (MW)	2
Heat Pump COP	3.72
Electrical Input Requirement (MW)	0.67

A process flow diagram for the Eavor-Loop, heat pump, and heat network is shown below assuming summer operating conditions. The heat pump will extract additional heat from the system prior to the working fluid entering the inlet wellbore. The heat that is extracted from the cold side will then be transferred to the hot side of the working fluid, and this will ensure that the working fluid temperature is always hotter than the heat network temperature. Additionally, by extracting heat from the cold side of the Eavor-Loop, the inlet temperature is lowered resulting in a larger temperature difference between the inlet and outlet wells, thereby increasing the thermal duty of the system.

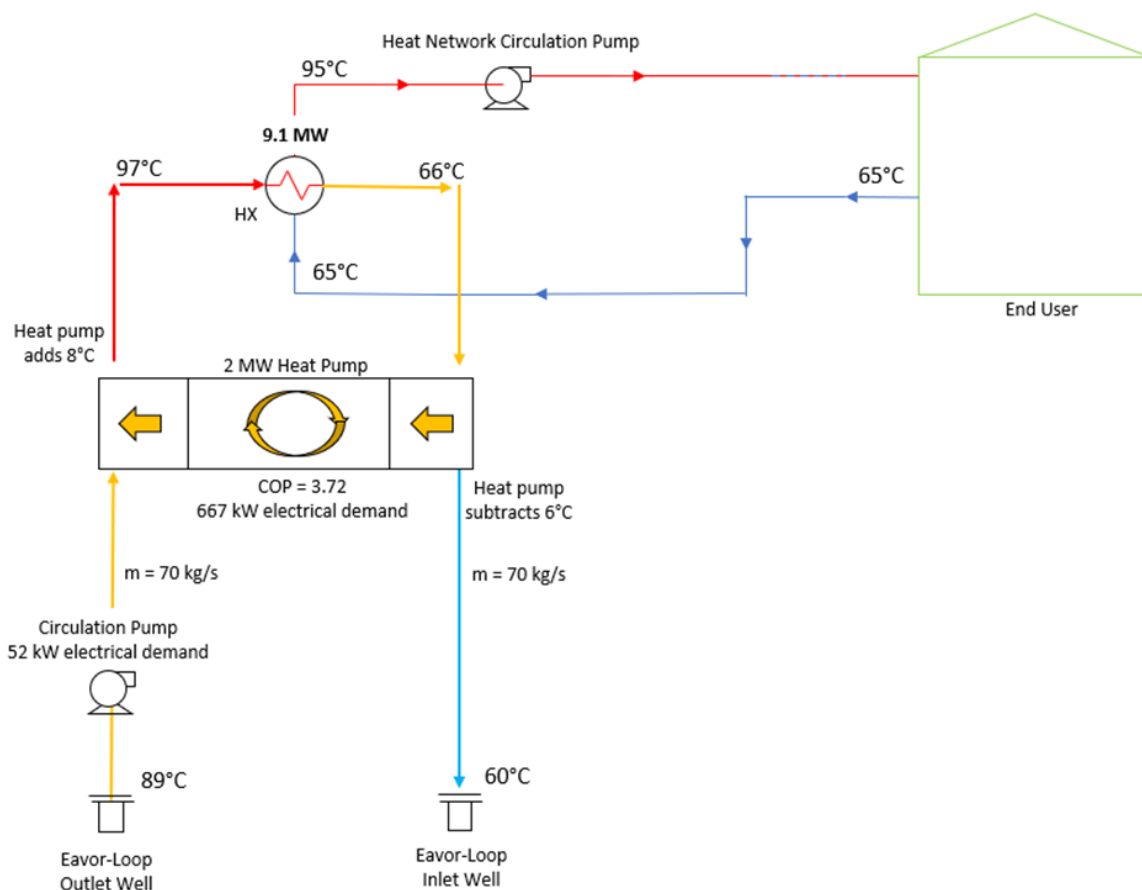


Figure 35: Process flow diagram – summer operations

## 2.9. Techno-Economic modelling

The Tilburg project projects to be the first implementation of an Eavor-Loop in the Netherlands. The development in Tilburg will follow the first commercial Eavor-Loop project in Geretsried, planned to spud in Mid-2023. Eavor-Loops are frequently modelled to a project life of 30 years, yet given the appropriate geological conditions described in the previous sections, it is possible for an Eavor-Loop

to have a much longer project life. Table 8 provides a summary of the main inputs used in the Project financial analysis, followed by a discussion on key input parameters.

Table 13: Financial Model Inputs and Outputs

<b>Construction</b>	
Capital Cost (€)	54,592,282
NWN! Grant (€)	10,000,000
<b>Production</b>	
P50 Summer Output (MW)	9.1
P50 Winter Output (MW)	7.1
Annual Runtime (hours)	8,584.8
Annual Production (MWh)	73,952.0
Project Life (years)	30.0
First Production	01-Jan-25
Last Production	31-Dec-54
<b>Operating Costs</b>	
Annual General Operating Costs (€)	161,800.0
Annual Power Consumption (MWh)	6,172.0

### P50 Output

A detailed discussion of the Project energy yield is provided in 2.8.3. The Summer Output represents the capacity of the system from April to December whereas the Winter Output represents the capacity of the system from January to March.

### Annual Runtime

The Project capacity factor (uptime) is 98%, driven by the availability and frequency of maintenance required for the surface equipment. The Eavor-Loops themselves do not require maintenance or downtime. Since the system can operate as a baseload source of heat, availability is limited by the availability of the surface equipment and not the resource itself. Eavor's modelling accounts for planned outages every 5 years, estimating a 20-day interval for the planned maintenance to occur for each of these periods. An additional 1% factor for unplanned outages is also applied on an annual basis. This factor is calculated on the productive hours excluding any durations of planned maintenance, as there is no risk of unplanned downtime while the facility is already offline for planned maintenance activities. The combination of planned outages and unplanned outages results in a 98% annual availability.

### Project Lifetime

Eavor-Loop assets are very long-lived and can remain productive for 100+ years with only a marginal decline in output (~0.2%/year) due to thermal interference between laterals beyond the 30-year design window (further detail is provided in Section 2.9). However, for the purposes of financial modelling a Project lifetime of 30-years is used as this is the duration over which the Eavor-Loop can operate with a flat output.

### 3. WP1 Discussion & Conclusions

The research carried out in WP1 has produced a robust prediction of the subsurface conditions near the City of Tilburg. Given the low uncertainty on Heat in Place it is possible to predict energy yield with relatively high confidence. To be able to predict energy yield prior to construction is one of the many benefits to developing high potential geothermal resources with the Eavor-Loop closed system.

The current location within the Attero energy park is suitable for Eavor-Loop deployment. It should be recognized that there are more preferred surface locations for subsurface deployment which have the potential to yield longer lateral lengths and approximately 20% higher energy yield. However, these locations are not viable due to population and nature protection areas and are excluded from Eavor-Loop development for the immediate future. In addition, the Tilburg Graben extends further to the North and additional grabens can be encountered as the Amer heating network continues West and North. These settings have the potential for future Eavor-Loop development and further heating grid decarbonization following successful deployment in the Tilburg city area.

In conclusion, the results of WP1 provide a feasible basis for Eavor-Loop development in the Tilburg city area. An Eavor-Loop can be deployed in the Lower German Triassic sandstone rich Volprieausen, Detfurth and Hardeggen members. An expected energy yield of 9.1 MW in summer months and 7.1 MW in the winter months yielding an approximate annual production of 74,000 MWh of clean baseload heating into the Amer heating network.

The remainder of the ELFO project will investigate the following topics:

- WP2 Optimized drilling rig design and drilling practices for EL lowering construction costs, reducing costs by 10-20% compared to conventional drilling.
- WP3 Environmental impact & safety assesses the environmental impact and safety of the EL. We aim to assess the value of environmental benefits of EL – no corrosion, no RA scales, no pumping energy, no leakage risks, and low risk of induced seismicity.
- WP4 System integration Eavor in district heating: the Eavor-Loop contains many engineering and operational parameters, which need to be tailored for system integration in heat networks. In this WP we will optimize the EL design towards district heating network integration, showcased for the Amer network.
- WP5 Outlook for NL and dissemination for wider implementation in the Netherlands. The research team would like to thank TKI for providing grant funding for this study.

The WP1 team would like to thank contributions from project partners and collaborators: Eavor, EBN, Ennatuurlijk, TNO, Huisman, Panterra, and RVO.

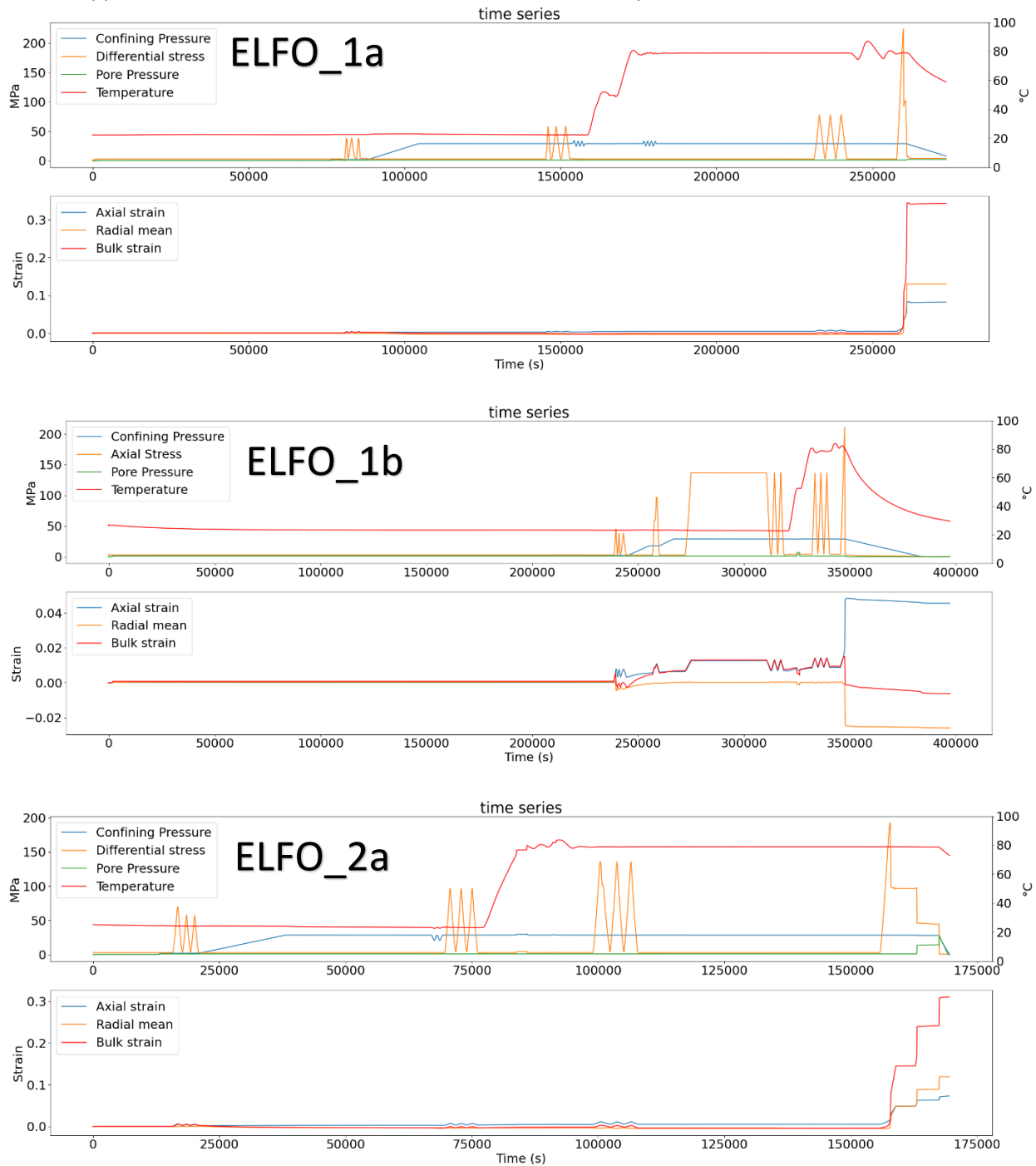
## 4. References

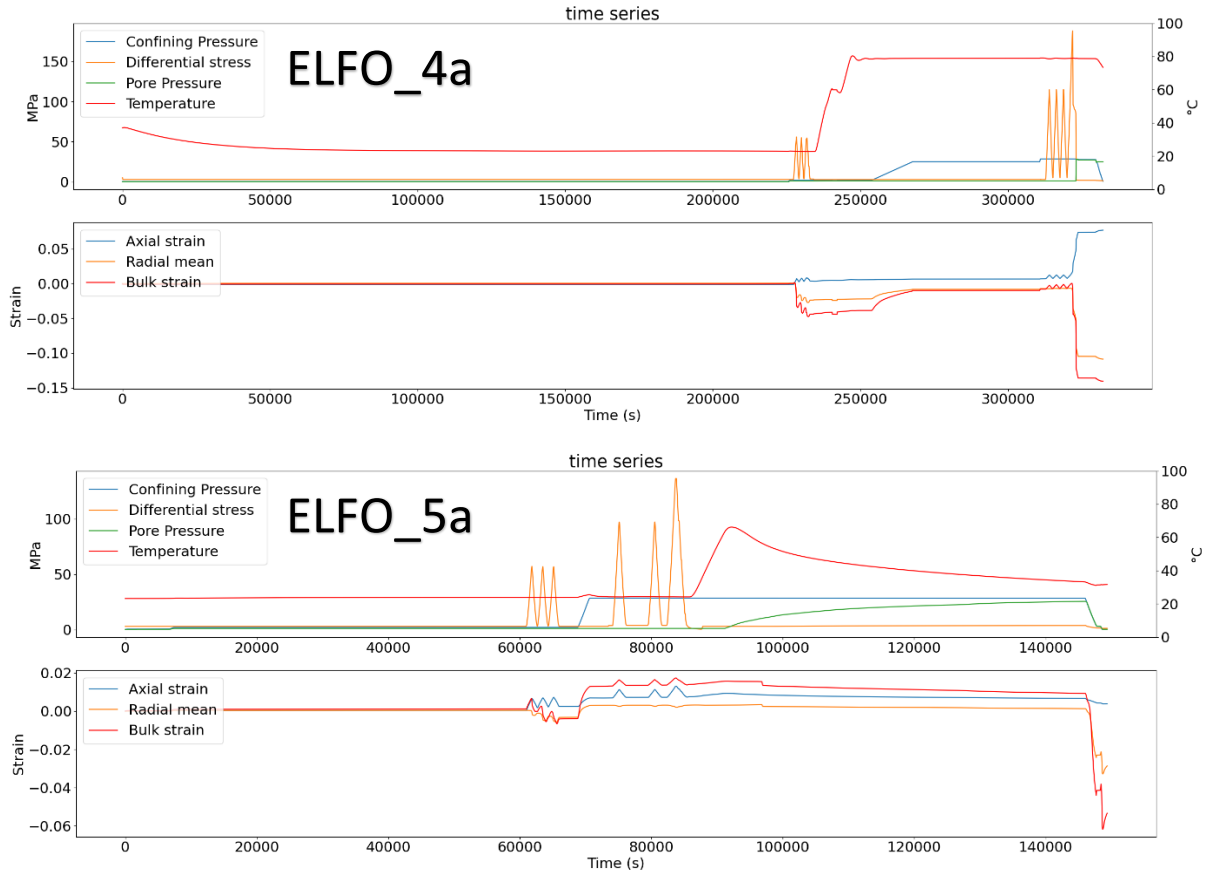
- Ames, R. & Farfan, P.F. 1996. The environment of deposition of the Triassic Main Buntsandstein Formation in the P and Q quadrants, offshore the Netherlands. In: Rondeel, H.E., Batjes, D.A.J. & Nieuwenhuijs, W.H. (eds): *Geology of gas and oil under the Netherlands*. Kluwer (Dordrecht), 167-178.
- ASTM, 2014. D 7012-14 standard test methods for compressive strength and elastic moduli of intact rock core specimens under varying states of stress and temperatures.
- Bakx, E., Wassing, B., Buijze, L., 2022. Formation, lithology and region-specific minimum horizontal stress field in the Netherlands: implications for fault stability in geothermal doublets.
- Camelbeeck, T., 1994. The 1992 Roermond earthquake, the Netherlands, and its aftershocks. *Geol. En Mijnbouw* 73 (2–4), 181–197.
- Camelbeeck, T., Van Eck, T., 1994. The Roer Valley Graben earthquake of 13 April 1992 and its seismotectonic setting. *Terra Nova* 6 (3), 291–300.
- Cermak, V. & Rybach, L. (1982) Thermal Conductivity and Specific Heat of Minerals and rocks. In: *Geophysics – Physical Properties of Rocks* (pp. 305-343).
- Carcione, J.M. & F. Cavallini, 2002. Poisson's ratio at high pore pressure. *Geophysical Prospecting*, 50(1), 97-106.
- Carcione, J.M., H.B. Helle, J.E. Santos & C.L. Ravazzoli, 2005. A constitutive equation and generalized Gassmann modulus for multimineral porous media. *Geophysics*, 70(2), N17-N26.
- Cloetingh, S., van Wees, J.D., Ziegler, P.A., Lenkey, L., Beekman, F., Tesauro, M., Worum, G., 2010. Lithosphere tectonics and thermo-mechanical properties: an integrated modelling approach for Enhanced Geothermal Systems exploration in Europe. *Earth-Sci. Rev.* 102 (3–4), 159–206.
- Dirkzwager, J.B., Wees, J.D.V., Cloetingh, S.A.P.L., Geluk, M.C., Dost, B., Beekman, F., 2000. Geo-mechanical and rheological modelling of upper crustal faults and their near-surface expression in the Netherlands. *Global Planet. Change* 27, 67.
- Dost, B., Goutbeek, F., Van Eck, T., Kraaijpoel, D., 2012. Monitoring induced seismicity in the North of the Netherlands: status report 2010. Report No. WR 2012-13. Royal Netherlands Meteorological Institute, De Bilt.
- Eck, T.v., Goutbeek, F., Haak, H., Dost, B., 2006. Seismic hazard due to small magnitude, shallow-source, induced earthquakes in the Netherlands. *Eng. Geol.* 87, 105.
- Fjaer, E., R.M. Holt, P. Horsrud & A.M. Raaen, 2008. *Petroleum related rock mechanics*: Elsevier.
- Gölke, M., Coblentz, D., 1996. Origins of the European regional stress field. *Tectonophysics* 266 (1–4), 11–24.
- Grünthal, G., Stromeyer, D., 1992. The recent crustal stress field in Central Europe: trajectories and finite element modeling. *J. Geophys. Res.* 97 (B8), 11,805.
- Heidbach, O., M. Rajabi, X. Cui, K. Fuchs, B. Müller, J. Reinecker, K. Reiter, M. Tingay, F. Wenzel, F. Xie, M. O. Ziegler, M.-L. Zoback, and M. D. Zoback. 2018, The World Stress Map database release 2016: Crustal stress pattern across scales. *Tectonophysics*, 744,484-498. <http://doi.org/10.1016/j.tecto.2018.07.007>
- Hackston, A. & E. Rutter, 2016. The Mohr–Coulomb criterion for intact rock strength and friction – a re-evaluation and consideration of failure under polyaxial stresses. *Solid Earth*, 7(2), 493-508.

- Heap, M.J., M. Villeneuve, A.R.L. Kushnir, J.I. Farquharson, P. Baud & T. Reuschlé, 2019. Rock mass strength and elastic modulus of the Buntsandstein: An important lithostratigraphic unit for geothermal exploitation in the Upper Rhine Graben. *Geothermics*, 77, 236-56.
- Hofstee, C., Benedictus, T., ter Heege, J., Huibregtse, J., van der Meer, B., Nelskamp, S., Orlic, B., Pluymaekers, M., Tambach, T., 2009. Feasibility of CO<sub>2</sub> storage in the Friesland platform. TNO-034-UT-2009-01084
- Kombrink, H., Doornenbal, J.C., Duin, E.J.T., Den Dulk, M., Van Gessel, S.F., Ten Veen, J.H., Witmans, N., 2012. New Insights into the geological structure of the Netherlands; results of a detailed mapping project. *Neth. J. Geosci.* 91 (4), 419–446.
- Lu, Y., W. Li, L. Wang, Z. Li, X. Meng, B. Wang & K. Zhang, 2019. Damage Evolution and Failure Behavior of Sandstone under True Triaxial Compression. *Geotechnical Testing Journal*, 42(3).
- Plenefisch, T., Bonjer, K., 1997. The stress field in the Rhine Graben area inferred from earthquake focal mechanisms and estimation of frictional parameters. *Tectonophysics* 275 (1–3), 71–97.
- Pluymaekers, M.P.D., Doornenbal, J.C., Middelburg, H., Velmod-3.1, TNO 2017 R11014 with erratum page 67 Final, 2017.
- Pijnenburg, R.P.J., B.A. Verberne, S.J.T. Hangx & C.J. Spiers, 2019. Inelastic Deformation of the Slochteren Sandstone: Stress - Strain Relations and Implications for Induced Seismicity in the Groningen Gas Field. *Journal of Geophysical Research: Solid Earth*, 124(5), 5254-82.
- Somerton, W.H., 1992. Chapter IV. Thermal Expansion of Rocks, in *Developments in Petroleum Science*, ed. W.H. Somerton. Elsevier, 29-38.
- Soustelle, V., J. ter Heege, L. Buijze & B. Wassing, In prep. Thermomechanical parameters of geothermal analogue reservoir sandstones in the West Netherlands Basin TNO.
- Toews, M. and Holmes, M. (2021): Eavor-Lite Performance Update and Extrapolation to Commercial Projects, Proceedings, Geothermal Rising Conference, California, USA (2021), vol. 45
- Van Adrichem Boogaert, H.A. & Kouwe, W.F.P. 1994. Stratigraphic nomenclature of The Netherlands; revision and update by RGD and NOGEP, Section E, Triassic. *Mededelingen Rijks Geologische Dienst*, 50, 1-28.
- Vucelic, L.A.B., K. Duffaut & P. Avseth, Burial induced changes in physical sandstone properties: A case study of North Sea and Norwegian Sea sandstone formations, in *SEG Technical Program Expanded Abstracts 2017*, 3626-31.
- Wang, J.C., 1984. Young's modulus of porous materials. *Journal of Materials Science*, 19(3), 801-8.
- Worum, G., van Wees, J., Bada, G., van Balen, R.T., Cloetingh, S., Pagnier, H., 2004. Slip tendency analysis as a tool to constrain fault reactivation: a numerical approach applied to three-dimensional fault models in the Roer Valley Rift system (Southeast Netherlands). *J. Geophys. Res.* 109, 02401.
- Zoback, M.D., Townend, J., 2001. Implications of hydrostatic pore pressures and high crustal strength for the deformation of intraplate lithosphere. *Tectonophysics*, 336, 19.

## Appendix A. Experimental data vs. Time

In this appendix, we show the time series records for all experiments as shown in section 2.3:





## Appendix B. Measured elastic Moduli for RBMV samples

Table Appendix B: Measured elastic Moduli for RBMV samples

Sample	Formation	T (°C)	Pe (MPa)	E <sub>s</sub> (GPa)	E <sub>s</sub> error (GPa)	V <sub>s</sub>	V <sub>s</sub> error
ELFO_1a	RBMVL	22	1.0	13.09	0.19	0.123	0.001
		22	1.0	13.66	0.11	0.138	0.001
		22	1.0	13.39	0.16	0.144	0.002
		22	28.0	24.89	0.07	0.056	0.002
		22	28.0	24.87	0.05	0.169	0.002
		22	28.0	24.88	0.05	0.186	0.002
		80	28.0	26.14	0.05	0.115	0.001
		80	28.0	26.08	0.05	0.120	0.001
		80	28.0	26.02	0.05	0.127	0.001
ELFO_1b	RBMVL	22	1.0	7.68	0.11	0.359	0.004
		22	1.0	7.70	0.12	0.264	0.001
		22	1.0	7.77	0.08	0.249	0.001
		22	28.0	22.06	0.08	0.045	0.000
		22	28.0	22.05	0.08	0.040	0.000
		80	28.0	23.48	0.08	0.055	0.000
		80	28.0	23.25	0.08	0.045	0.000
		80	28.0	23.36	0.08	0.044	0.000
ELFO_2b	RBMVL	22	1.0	14.20	0.15	0.119	0.001
		22	1.0	12.97	0.15	0.165	0.001
		22	1.0	16.73	0.12	0.175	0.001
		22	27.7	21.55	0.08	0.137	0.000
		22	27.7	22.26	0.08	0.146	0.000
		80	27.7	21.62	0.07	0.151	0.151
		80	27.7	22.29	0.08	0.180	0.180
ELFO_4a	RBMVU	22	1.0	12.10	0.12	-	-
		22	1.0	12.15	0.13	-	-
		22	1.0	12.15	0.12	-	-
		80	27.5	22.81	0.08	0.145	0.000
		80	27.5	22.73	0.08	0.136	0.000
		80	27.5	22.81	0.08	0.148	0.000
ELFO_5a	RBMVU	22	1.0	10.75	0.12	0.223	0.009
		22	1.0	11.64	0.12	0.292	0.017
		22	1.0	11.76	0.12	0.280	0.018
		22	27.4	23.09	0.06	0.127	0.000
		22	27.4	23.09	0.06	0.150	0.001
		22	27.4	23.32	0.06	0.219	0.000